

Written: December 1969  
Distributed: March 31, 1970

LA-4097-MS  
UC-34, PHYSICS  
TID-4500

**LOS ALAMOS SCIENTIFIC LABORATORY**  
**of the**  
**University of California**  
LOS ALAMOS • NEW MEXICO

**Thick Target Bremsstrahlung Theory**



by

C. Robert Emigh





## CONTENTS

Foreword .....	iv
Abstract .....	1
Chapter	
I. A THICK TARGET ON-AXIS BREMSSTRAHLUNG THEORY .....	3
A. Problem Formation and Geometric Considerations .....	3
B. Multiple Scattering .....	6
C. Bremsstrahlung Angular and Energy Distributions .....	8
D. Bremsstrahlung Weighting Function - the $\theta$ Integral .....	9
E. Bremsstrahlung Energy Distribution-Approximation .....	13
F. Summary .....	17
II. THICK TARGET OFF-AXIS BREMSSTRAHLUNG THEORY .....	21
A. Geometric Considerations .....	21
B. Weighting Function .....	21
C. The Weighting Function - An Approximation .....	27
D. Thick Target Bremsstrahlung .....	28
E. Optimum Target Thickness .....	29
F. Angular Intensity Distribution for Optimum Target .....	32
G. Variation of the Spectral Distribution with Angle .....	32
H. Summary .....	32
III. IMPROVEMENTS IN DEVELOPMENT OF OFF-AXIS BREMSSTRAHLUNG THEORY.	36
A. Improved Approximations .....	36
B. Experimental Verification .....	44
C. Summary .....	52
APPENDIX A. B - Approximation .....	56
APPENDIX B. Effective Depth of Bremsstrahlung Generation .....	58
APPENDIX C. Optimum Thickness .....	60

APPENDIX D. Exponential Integral Approximation .....	62
APPENDIX E. Useful Data .....	64
APPENDIX F. Calculation of $\bar{a}$ .....	65
APPENDIX G. Effective Depth of Bremsstrahlung Generation .....	67
APPENDIX H. Nomenclature .....	68
Acknowledgments .....	71
References .....	72

## FOREWORD

The following manuscript was originally formulated over a number of years as three separate memoranda. Because of the interest in the development of the theory of thick target bremsstrahlung from high-energy electrons ( $> m_0 c^2$ ) for radiographic purposes, these memoranda are reproduced as three separate chapters in essentially their original form. The final result is developed in Chapter VIII, Eq. (96), with the subsequent approximations being more useful depending upon the geometry of the problem. Although the work covered in Chapter III is preempted by the development in Chapter VIII, it is included in this manuscript because of its value in the later generation of the more accurate approach. The nomenclature used is defined in Appendix II and, where applicable, the source is noted.

## ABSTRACT

Chapter I contains the calculations for thick target bremsstrahlung in the forward direction. The theory presented is complete with regard to such details as multiple electron scattering, electron-energy degradation in the target, bremsstrahlung angular distribution, variation of bremsstrahlung distribution with a decreasing electron energy, and target self-absorption. Past theories have accounted for some, but not all, of these effects. The approximations presented here are for heavy elements, particularly tungsten; they should also apply to the lighter elements but perhaps not with the same degree of accuracy.

Chapter II covers for the off-axis theory the same details presented in Chapter I for the on-axis theory. It accounts for the angular displacement of the detector from the axis. The off-axis theory is useful in determining the optimum target-object distance for certain densitometric or radiographic observations. The distinguishing characteristics of this theory are that it is continuous for all thicknesses of target, zero to infinity; it is continuous for detector angle displacements, zero to values greater than the half-intensity angle; and it introduces a new energy-dependent parameter  $t'$ , which is the lesser of either thickness or the distance traveled by an electron in the target and emitting a photon of energy  $k$  at the end of its range.

Chapter III presents improvements in the development of the off-axis theory covered in Chapter II including the effects of plural scattering, the transitional region between multiple and single scattering. The need for such improvements was indicated by the discrepancy between previous off-axis theories and the published experimental results. A surprising result is that terms added to account for plural scattering contribute only negligibly to the angular radiation distribution, which is in

contrast to predictions. The long tail to the angular distribution is primarily a result of the convolution of the multiple-scattering angular distribution and the bremsstrahlung angular distribution. A weighting function is developed and compared with the experimental results; agreement with theory is within the experimental error.

## CHAPTER I

### A THICK TARGET ON-AXIS BREMSSTRAHLUNG THEORY

#### A. Problem Formation and Geometric Considerations

The first assumption made is that all the electrons in the incident beam are normal to the target. In practice, this usually is not the case, but the effect is small and tends to reduce the on-axis intensity according to the angular distribution of the incident electrons. The effect on the bremsstrahlung energy distribution is correspondingly small. In Fig. 1, the electron beam is incident upon a target of thickness  $t$ . At the depth  $x$ , radiation is produced in the differential thickness  $dx$ , and a small portion of this radiation will reach an on-axis detector.

Consider the electrons which strike the element  $dx$  at a depth  $x$  and with an angle  $\theta_e$ . In this theory, all energies are considered to be relativistic and all angles of importance are assumed to be small; for example  $\sin \theta_e = \theta_e$ . The fractional number of electrons having the direction  $\theta_e$  at the depth  $x$  will be expressed as  $f(\theta_e, x, E_0) \theta_e d\theta_e$ . The differential bremsstrahlung intensity per steradian that will reach the detector will be

$$dI(k, x, \theta_e, \theta_\gamma) = \frac{nNk}{\rho} f(\theta_e, x, E_0) \theta_e d\theta_e S(k, x, \theta_\gamma, E_0) dxdk, \quad (1)$$

where  $S(k, x, \theta_\gamma, E_0)$  is the differential bremsstrahlung cross section. Because this is a cylindrically symmetrical theory, the usual third dimension,  $d\phi_e$ , need not be explicitly considered.

The differential intensity per steradian reaching the detector, integrated over all possible angles  $\theta_e$ , is

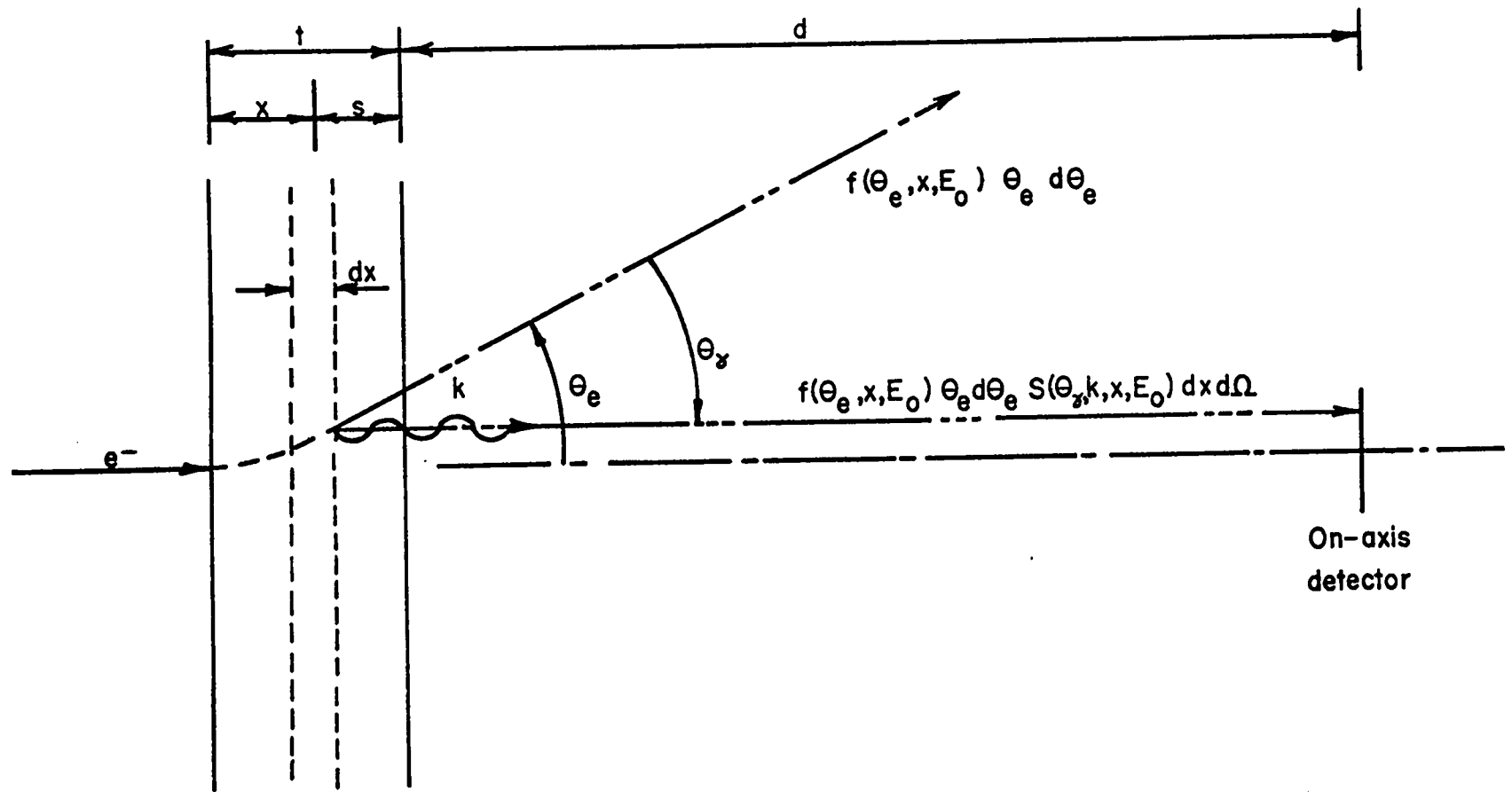


Fig. 1. Thick target geometry.

$$dI(k,x) = \frac{nNk}{\rho} \int_{\theta_e=0}^{\infty} f(\theta_e, x, E_0) \theta_e d\theta_e S(k, x, \theta_\gamma, E_0) dx dk. \quad (2)$$

Integration over the  $\theta_e$  parameter is taken to infinity as a mathematical convenience, but no practical error will result because the integrand rapidly approaches zero as  $\theta_e$  increases past  $10^\circ$  for our range of investigation. Not included in the above formulation is the self-absorption of the produced gamma rays as they penetrate the remainder of the target,  $s$ . To account for this, the simple narrow-beam absorption coefficient  $\mu(k)$  is used. The intensity becomes

$$dI(k,x) = \frac{nNk}{\rho} \int_{\theta_e=0}^{\infty} f(\theta_e, x, E_0) S(k, x, \theta_\gamma, E_0) \exp\{-\mu(k)s\} \theta_e d\theta_e dx dk. \quad (3)$$

The intensity, as seen by a perfect on-axis detector from a target of thickness  $t$ , is given as a function of the photon energy,  $k$ .

$$dI(k,t) = \frac{nNk}{\rho} \int_{x=0}^t \int_{\theta_e=0}^{\infty} f(\theta_e, x, E_0) S(k, x, \theta_\gamma, E_0) \exp\{-\mu(k)s\} \theta_e d\theta_e dx dk. \quad (4)$$

This expression can be simplified from geometric considerations if the detector is far from the target and is small in size. Then, as  $d \gg t$ , the electrons that are deflected by an angle  $\theta_e$  at the depth  $x$  must produce photons at the angle  $\theta_\gamma = \theta_e$  for the detector to respond. Thus, the simplification is made that  $\theta_\gamma = \theta_e = \theta$ , and the intensity per steradian is expressed by

$$dI(k,t) = \frac{nNk}{\rho} \int_{x=0}^t \int_{\theta=0}^{\infty} f(\theta, x, E_0) S(k, x, \theta, E_0) \exp\{-\mu(k)s\} \theta d\theta dx dk. \quad (5)$$

Equation (5) is the formulation of our basic problem and will be solved in several steps in the next few sections.

### B. Multiple Scattering

The multiple scattering as a function of the depth  $x$  is given by the function  $f(\theta, x, E_0)$  in Eq. (5). The most accurate account of this fractional electron distribution is given by the Molière theory.<sup>1</sup> Only the first term, which is Gaussian and normalized, is used and is quite accurate for our purpose. The error is less than 2% in relative magnitude as a function of angle.

$$f(\theta, x, E_0) = \frac{2}{\theta_1^2 B} \exp\left\{-\theta^2 / \theta_1^2 B\right\}, \quad (6)$$

where  $\theta_1^2$ <sup>2</sup> and  $B$  are constants for the  $\theta$  integration.

#### 1. $\theta_1^2$ Evaluation.

The theory departs from the usual treatment to include the effect of the electron energy decreasing with target penetration. The relativistic Mott<sup>2</sup> formula for scattering, but neglecting screening, is used as the basic equation,

$$f_m(\theta, x, E_0) d\theta dx = \frac{K d\theta dx}{x \epsilon^2 \theta^3 \mu^2}, \quad (7)$$

where

$$K_1 = 8\pi NZ(Z+1)z^2 e^4.$$

The parameters involved are defined by Segrè.<sup>3</sup> The assumption is now made that the kinetic energy of the electrons at the depth  $x$  is

$\mathcal{E}_x = \mathcal{E}_0 g(x)$ , where  $g(x)$  is a monotonically decreasing function of the thickness.  $\theta_1^2$  is defined in such a way that many collisions occur in

the foil for  $\theta < \theta_1$ , but not many occur for  $\theta > \theta_1$ . In particular, only one collision occurs for all angles greater than  $\theta_1$ . The probability of a collision occurring at the angle  $\theta$  in the thickness  $x$  will be

$$P_c = \int_0^x f_m(\theta, x, \mathcal{E}_0) d\theta dx,$$

or

$$P_c = K_1 f(x) d\theta / \theta^3 \mathcal{E}_0^2 \mu^2, \quad \text{where } f(x) = \int_0^x g^{-2}(x) dx. \quad (8)$$

This probability,  $P_c$ , is set equal to unity for all angles  $\theta > \theta_1$ , that is,

$$1 = \int_{\theta_1}^{\infty} \frac{K_1 f(x) d\theta}{\theta^3 \mathcal{E}_0^2 \mu^2}. \quad (9)$$

When solved for  $\theta_1$ ,

$$\theta_1^2 = K_1 f(x) / 2\mu^2 \mathcal{E}_0^2. \quad (10)$$

## 2. B Evaluation.

The B parameter is rather complicated. However, B can be accurately approximated by the following function where the error is less than 1% for the entire range of interest.

$$B \approx \ln \left\{ 1.1 \zeta^2 \ln 1.4 \xi^2 \right\}, \quad (11)$$

where

$$\zeta^2 = 7800 \frac{Z^{\frac{1}{3}}(Z+1)z^2 f(x)}{A(1+3.35 \alpha^2)}$$

Again, the nomenclature used in this formula is that used by Segrè.<sup>3</sup> The approximation in Eq. (11) is developed by a simple perturbation theory and is presented in Appendix A.

## C. Bremsstrahlung Angular and Energy Distributions.

Schiff<sup>4</sup> has developed the following formula for intrinsic bremsstrahlung intensity at small angles from the direction of the incident electron beam.

$$S(k, \theta, E_x) = \frac{2Z^2 r_o^2 E_x^2}{137\pi k} \left\{ \frac{16\theta^2 E E_x}{(1+\theta^2 E_x^2)^4} - \frac{(E_x + E)^2}{(1+\theta^2 E_x^2)^2 E_x^2} \right. \\ \left. + \left[ \frac{E^2 + E_x^2}{(1+\theta^2 E_x^2)^2 E_x^2} - \frac{4\theta^2 E_x E}{(1+\theta^2 E_x^2)^4} \right] \ln M(k, \theta, E_x) \right\}, \quad (12)$$

where

$$M^{-1}(k, \theta, E_x) = \left( \frac{k}{2E_x E} \right)^2 + \left( \frac{Z^{\frac{1}{3}}}{111(E_x^2 \theta^2 + 1)} \right)^2.$$

The only photons that will survive to contribute significantly to the total intensity, because of the double process of multiple scattering and bremsstrahlung, are those whose angle  $\theta$  is less than the order of  $\epsilon_0^{-1}$ . Using this as a basis, Schiff's equation can be further simplified and the variables separated:

$$S(k, \theta, E_x) dk \theta d\theta = S_1(k, E_x) dk S_2(\theta, E_x) \theta d\theta, \quad (13)$$

where  $S_1$  is the energy distribution evaluated for  $\theta = 0$ ,

$$S_1(k, E_x) dk = \frac{2Z^2 r_0^2}{137\pi} \left\{ \frac{(E^2 + E_x^2)}{E_x^2} \ln M(k, \theta, E_x) - \frac{(E + E_x)^2}{E_x^2} \right\} \frac{E^2 dk}{k}, \quad (14)$$

and  $S_2$  is the angular distribution

$$S_2(\theta, E_x) = \left[ 1 + E_x^2 \theta^2 \right]^{-2}. \quad (15)$$

#### D. Bremsstrahlung Weighting Function - the $\theta$ Integral

##### 1. Exact Expression.

The foregoing section has separated the variables  $k$  and  $\theta$ , and now it is desirable to evaluate the  $\theta$  integral. Gathering all the functions related to  $\theta$ , that is,  $f(\theta, x, E_0)$  and  $S_2(\theta, E_x)$ , the  $\theta$  integral becomes

$$W(x, E_0) = \int_{\theta=0}^{\infty} f(\theta, x, E_0) S_2(\theta, E_x) \theta d\theta, \quad (16)$$

where  $W(x, E_0)$  can be interpreted as the weighting function for the production of bremsstrahlung at the depth  $x$  of the target per unit solid angle of

the detector. Substituting Eqs. (6) and (15) into Eq. (16), the weighting function becomes

$$W(x, E_0) = \int_{\theta=0}^{\infty} \alpha^2 (\alpha + \theta^2)^{-2} 2p \exp\{-p\theta^2\} \theta d\theta, \quad (17)$$

where

$$\alpha = E_x^{-2}, \quad p = 1/B\theta_1^2.$$

Fortunately, this integral is directly reducible as a Laplace transformation and yields for the weighting function

$$W(x) = \left[ \alpha p + \alpha^2 p^2 \exp(\alpha p) E_1(-\alpha p) \right], \quad (18)$$

where  $E_1(-\alpha p)$  is the exponential integral.

## 2. Approximate Expression.

The weighting function has already become a complicated function of thickness  $x$  and with the target thickness integration to perform, it would be convenient to express Eq. (18) in terms of directly integrable functions. By using the usual approximation for  $g(x)$ ,

$$g(x) = \frac{1}{\epsilon_0 B} \left[ (\sigma + \beta \epsilon_0) \exp(-\beta x) - \sigma \right], \quad (19)$$

and its derived counterpart

$$f(x) = \frac{\epsilon_0}{\sigma} \left[ g^{-1}(x) + \frac{\epsilon_0 \beta}{\sigma} \ln g(x) + \frac{\beta^2 \epsilon_0}{\alpha} x - 1 \right], \quad (20)$$

where  $\sigma$  is the intercept on the ordinate, and  $\beta$  is the slope of the

electron differential energy loss vs incident kinetic energy curve for tungsten, the weighting function,  $W(x)$ , has been graphed as a function of thickness,  $x$ , (Fig. 2). It is fortuitous, but not surprising, that  $W(x)$  is closely related to the form

$$W(x) \approx (1 + ax)^{-1}. \quad (21)$$

Here  $a$  is a constant. This form has the advantage of being a sectionally rational function that is Laplace transformable, leading to the spectral distribution in a closed form. This and other similar expressions have been derived by other authors<sup>5,6,7</sup> through the use of many rough approximations. The main approximations are: (1) the energy of the electron is not degraded in its travel through the target, and (2) the bremsstrahlung angular distribution is of a type that can be represented by a series of Gaussian terms. The accuracy of the expression in Eq. (21) is far better than these approximations would lead one to expect as the errors are largely self-canceling over the  $\theta$  integration.

In order to use the expression in Eq. (21), the constant  $a$  must be evaluated. The best fit for the approximate expression to the exact expression should be evaluated in the region of interest, that is, in the region of the effective depth,  $\tau$  (Appendix B).

$$W(\tau) = (1 + a\tau)^{-1} = \alpha p + \alpha^2 p^2 \exp\{\alpha p\} E_1(-\alpha p), \quad (22)$$

where  $\alpha p$  is evaluated at  $\tau$ . Thus,

$$a = \left( \frac{1}{W(\tau)} - 1 \right) / \tau. \quad (23)$$

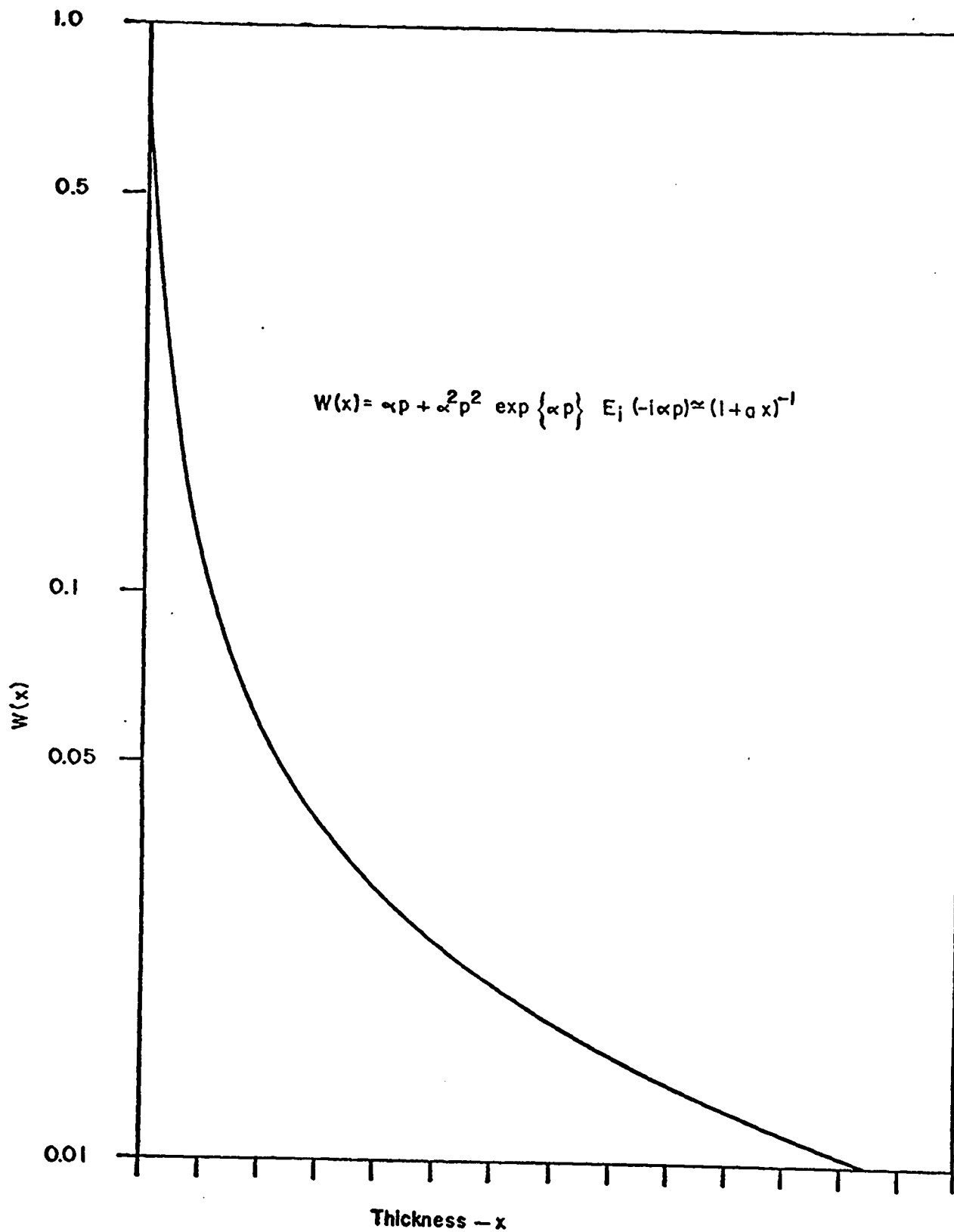


Fig. 2. Bremsstrahlung weighting function.

Using the value of the effective depth,  $0.06 \text{ g/cm}^2$ , the value of  $a$  for tungsten is  $165.3 \text{ cm}^2/\text{g}$ .

### E. Bremsstrahlung Energy Distribution-Approximation

#### 1. At Depth $x$ .

From the preceding section, and in reference to Appendix C, it is evident that the useful bremsstrahlung from a thick target is generated in a very thin layer near the front and the effective depth, in terms of energy degradation, is very small. Some authors have assumed no energy distribution variation with depth. However, although half the intensity is generated at a depth less than the effective depth,  $\tau$ , the other half is generated between  $\tau$  and at least as deep as the optimum depth,  $\tau_0$ . Therefore, a penetration correction is made to the distribution even though it may at first appear to be slight.

Equation (13) allows removal of the angular dependence from the spectral distribution. The energy distribution function  $S_1(k, E_x)$ , which is evaluated for  $\theta = 0$ , is left. Again, to ease the complicated  $x$ -integration yet to be performed, the function  $S_B(k, E_x)$ , which is the bracketed portion of  $S_1(k, E_x)$  in Eq. (14), is represented by

$$S_B(k, E_x) = S_B(k, E_0) \exp\{\Delta(k)x\}, \quad (24)$$

where  $\Delta(k)$  is a function to be determined. Because of the extremely sharp weighting function,  $W(x)$ , in the region of very small  $x$ , Eq. (24) may be solved for  $\Delta(k)$  as  $x \rightarrow 0$

$$\Delta(k) \underset{x \rightarrow 0}{=} \Delta(k) = \frac{dS_B(k, E_x)}{dE_x} \frac{1}{S_B(k, E_0)} \frac{dE_x}{dx}, \quad (25)$$

making  $\Delta(k)$  independent of  $x$ , but a function of energy  $k$ .

2. Thick Target.

Using the above expression and inserting it and  $W(x)$  from Eq. (21) into Eq. (5), the measured intensity distribution is

$$dI(k,t) = \frac{nNTk}{\rho} \int_{x=0}^{t'} \frac{1}{(1+ax)} E_x^2 S_B(k, E_0) \exp\{\Delta(k)x - \mu(k)s\} dx dk, \quad (26)$$

where

$$T = \frac{2Z^2 r_0^2}{137\pi}.$$

The upper limit,  $t'$ , replaces  $t$  to account for zero contribution from the spectral distribution for photon energies  $k > \epsilon_x$  at depth  $x$ . The function  $t'$  is derived as follows:

inasmuch as 
$$g(x) = \frac{1}{\epsilon_0 \beta} \left[ (\sigma + \beta \epsilon_0) \exp\{-\beta x\} - \sigma \right],$$

then 
$$k < \frac{1}{\beta} \left[ (\sigma + \beta \epsilon_0) \exp\{-\beta x\} - \sigma \right]$$

or, which is equivalent,

$$x < \frac{1}{\beta} \ln \left\{ \frac{\sigma + \beta \epsilon_0}{\sigma + \beta k} \right\}. \quad (27)$$

Thus, the upper limit will be  $\beta^{-1} \ln \left[ (\sigma + \beta \epsilon_0) / (\sigma + \beta k) \right]$  or  $t$ , whichever is smaller. To formalize,

$$t' = t \text{ for } t < \beta^{-1} \ln \left\{ \frac{\sigma + \beta \mathcal{E}_0}{\sigma + \beta k} \right\},$$

and

$$t' = \beta^{-1} \ln \left\{ \frac{\sigma + \beta \mathcal{E}_0}{\sigma + \beta k} \right\} \text{ for } t > \beta^{-1} \ln \left\{ \frac{\sigma + \beta \mathcal{E}_0}{\sigma + \beta k} \right\}. \quad (28)$$

For the purpose of evaluating the integral in Eq. (25), Eq. (26) can be considerably simplified. The justification for this comes from the very shallow effective depth indicating that, for the most part, the bremsstrahlung will be formed by electrons of nearly the same energy as the impinging electrons. Thus,

$$g(x) = \frac{1}{\mathcal{E}_0 \beta} \left[ (\sigma + \beta \mathcal{E}_0) \exp\{-\beta x\} - \sigma \right] \approx \exp\{-\xi x\}, \quad (29)$$

where

$$\xi = \beta + \sigma/\mathcal{E}_0.$$

Therefore,

$$\mathcal{E}_x \approx \mathcal{E}_0 \exp\{-\xi x\} \text{ and } E_x \approx E_0 \exp\{-\xi x\}. \quad (30)$$

Making the substitutions indicated by Eq. (30), and that allowed by  $x = t - s$ , the intensity becomes

$$dI(k, t) = \frac{nNk}{a \rho} S_1(k, E_0) e^{-\mu(k)t} \int_{x=0}^{t'} \frac{a}{1 + ax} \exp\{(\Delta + \mu - 2\xi)x\} dx dk,$$

where

$$\Delta = - \frac{dS_B(k, E_0)}{dE_0} \frac{\xi E_0}{S_B(k, E_0)} = - \frac{\xi E_0^3}{S_1(k, E_0)} \frac{d}{dE_0} \left\{ \frac{S_1(k, E_0)}{E_0^2} \right\}. \quad (31)$$

Fortunately, this can be reduced directly as a Laplace transformation and yields for the spectral distribution

$$dI(k, t) = \frac{nNk}{a \rho} S_1(k, E_0) \exp\{-\mu(k)t\} \exp\left\{(2\xi - \mu - \Delta) \frac{1}{a}\right\} \left\{ E_1\left[-\left(\frac{1}{a} + t'\right)(2\xi - \mu - \Delta)\right] - E_1\left[-\left(\frac{1}{a}\right)(2\xi - \mu - \Delta)\right] \right\} dk. \quad (32)$$

This differential intensity is expressed in units of  $m_0 c^2$ .

The above expression can be simplified and expressed by more familiar functions. First,  $(2\xi - \mu - \Delta) \frac{1}{a} \ll 1$ , so that the exponential of this argument can be equated to unity. Second, the exponential integrals can be expanded and combined into functions of natural logarithms to an accuracy greater than 0.1% for the region from zero to several times optimum thickness, and to better than 2.2% for any thickness. That is,

$$E_1\left[\left(\frac{1}{a} + t'\right)(\Delta + \mu - 2\xi)\right] - E_1\left[\left(\frac{1}{a}\right)(\Delta + \mu - 2\xi)\right] \\ \approx \ln(1 + at') - 2 \ln\left(1 + \frac{1}{2} at' (2\xi - \mu - \Delta)\right). \quad (33)$$

See Appendix D for a derivation of this approximation.

Making these substitutions,

$$dI(k, t) = \frac{nNk}{a \rho} S_1(k, E_0) e^{-\mu(k)t} \left\{ \ln(1 + at') - 2 \ln\left(1 + \frac{1}{2} at' (2\xi - \mu - \Delta)\right) \right\} dk, \quad (34)$$

where

$$D = 2\xi - \mu(k) - \Delta(k).$$

The essential characteristic of the distribution is given by the first term

$$dI(k,t) = \frac{nNk}{a \rho} S_1(k, E_0) e^{-\mu(k)t} \ln(1+at'), \quad (35)$$

and is sufficient for rough approximations (approximately 10 to 20% too high, depending on  $k$ ); however, the correction term, containing  $\Delta(k)$ , can contribute considerable detail, especially in the region where  $k \rightarrow E_0$ .

#### F. Summary

The important result contained in the expression in Eq. (34) gives the spectral distribution as seen by a detector far from the bremsstrahlung generating target of a given thickness,  $t$ . The theory is complete in that it is valid for any thickness of target from zero to  $\infty$ . It is difficult to attach an error specification to the equation. However, all the approximations are good to a few percent. Many of the approximations have little effect on the final results, and it is felt, in developing the theory, that the overall equation should be accurate to better than 3 or 4%.

Also of great interest is the optimum target thickness which should be used to generate the maximum intensity at the detector after the x rays have traversed a thick piece of some high-Z material. Figure 3 gives the spectral distribution from a tungsten target of optimum thickness,  $2.08 \text{ g/cm}^2$ . Also, for comparison, the differentially thin target spectrum is displayed.

Figure 4 shows a plot of the 3.5 MeV bremsstrahlung intensity as a

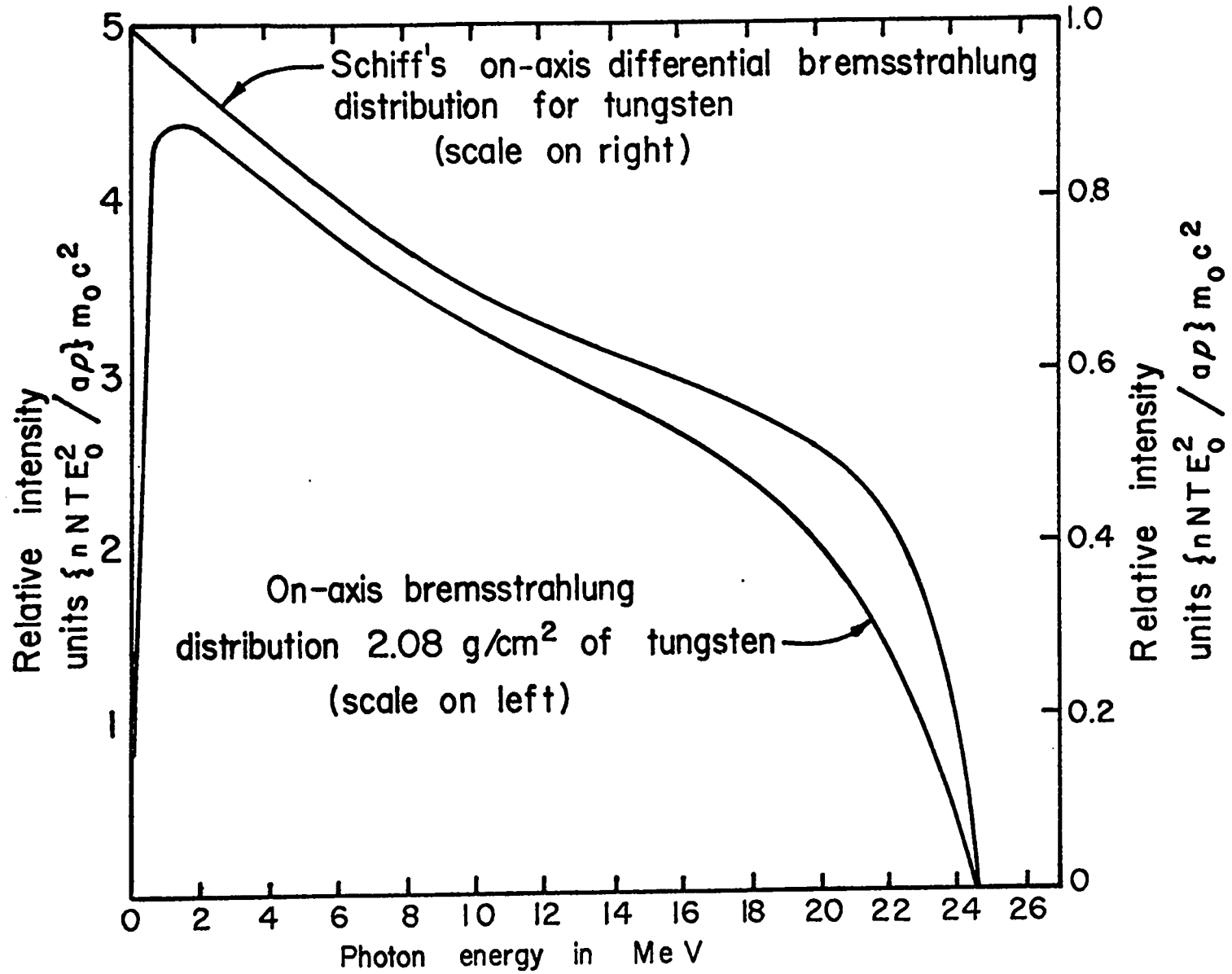


Fig.3. Bremsstrahlung intensity distributions .

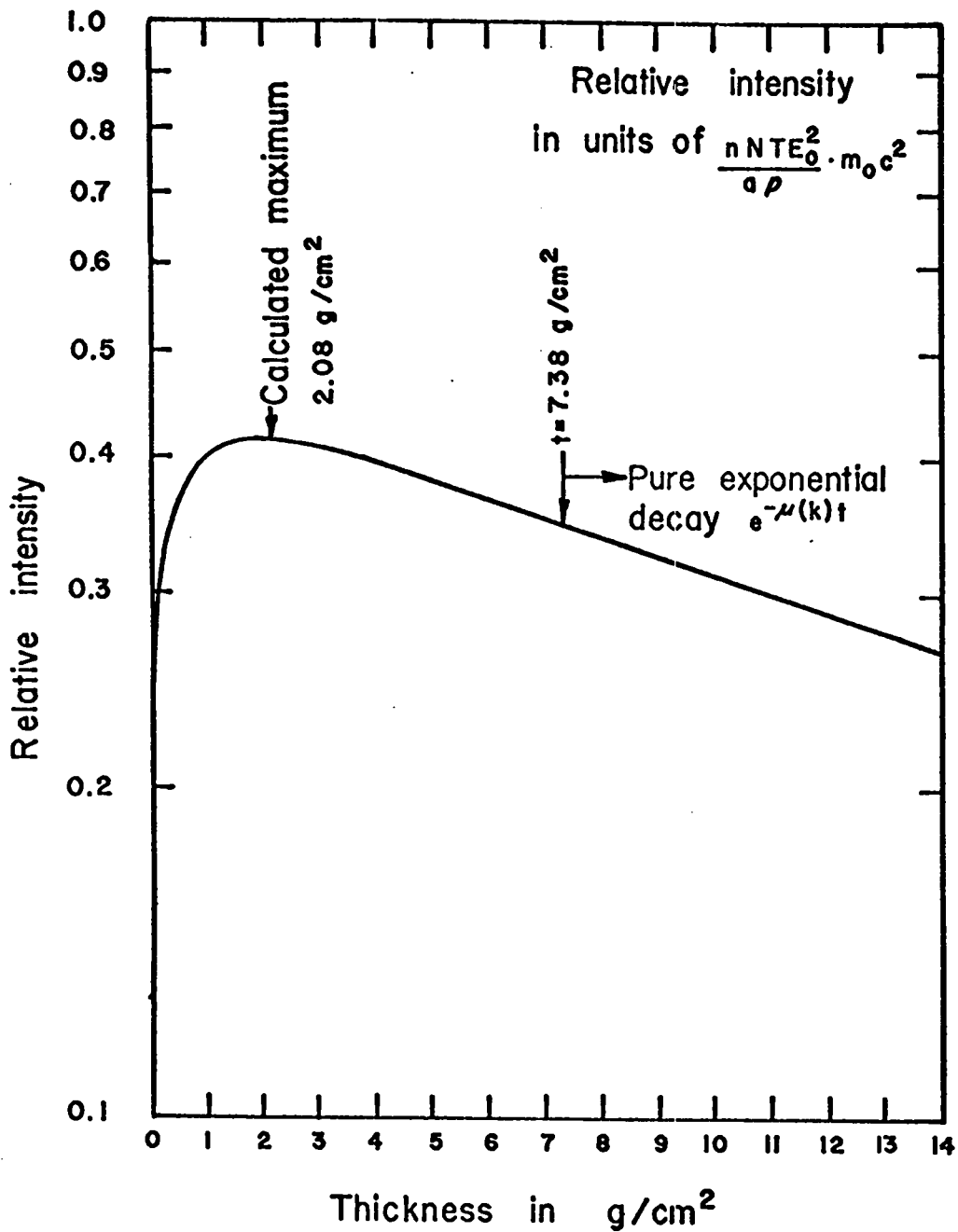


Fig 4. 3.5 MeV bremsstrahlung intensity vs tungsten target thickness.

function of tungsten target thickness. Because it is near the minimum absorption region for most high-Z materials, 3.5 MeV was chosen. The curve for the total intensity vs thickness would be slightly different because of the energy dependence of the various parameters such as absorption coefficient, spectral distribution, etc. Once the tungsten target thickness increases past  $7.38 \text{ g/cm}^2$ , the only detected influence on the bremsstrahlung is an exponential decay due to absorption because the electrons have been completely stopped at this depth. The parameter  $t'$  accounts for this effect.

It is interesting that the effective depth is so shallow compared to the optimum depth. This gives justification for not ignoring the penetration effects, namely, scattering, energy degradation, bremsstrahlung angular dependence, and self-absorption.

## CHAPTER II

### THICK TARGET OFF-AXIS BREMSSTRAHLUNG THEORY

#### A. Geometric Considerations

As in the on-axis theory, the electrons in the incident beam are assumed normal to the target. Figure 5 indicates the off-axis geometry where  $\theta_d$  is the angular displacement in radians of the detector,  $\theta_e$  is the angular displacement of the scattered electron at the depth  $x$ , and  $\theta_\gamma$  is the angular displacement of the emitted gamma ray relative to the emitting electron.

If one assumes that  $\theta_d$ ,  $\theta_e$ , and  $\theta_\gamma$  are all small compared to a unit radian, then

$$\theta_\gamma^2 = \theta_d^2 + \theta_e^2 - 2\theta_e \theta_d \cos \varphi, \quad (36)$$

where  $\varphi$  is the angle between the plane containing the axis and the scattered electron and the plane containing the axis and the emitted gamma ray.

#### B. Weighting Function

Equation (17) can be rewritten in terms of the newly defined angles. All development prior to Eq. (17) is valid for the off-axis analysis.

$$W(x, E_0, \theta_d) = \int_{\theta_e=0}^{\infty} \frac{1}{\pi} \int_{\varphi=0}^{\pi} \frac{\alpha^2}{(\alpha + \theta_\gamma^2)^2} 2p \exp\{-p\theta_e^2\} \theta_e d\theta_e d\varphi. \quad (37)$$

Substituting Eq. (36) into Eq. (37) and carrying out the indicated  $\varphi$  integration,

$$W(x, E_0, \theta_d) = \int_{\theta_e=0}^{\infty} \frac{\left(1 + \frac{\theta_d^2}{\alpha} + \frac{\theta_e^2}{\alpha}\right) p \exp\{-p\theta_e^2\}}{\left[1 + \frac{2\theta_d^2}{\alpha} + \frac{\theta_d^4}{\alpha^2} + 2\frac{\theta_e}{\alpha} \left(1 - \frac{\theta_d^2}{\alpha}\right) + \frac{\theta_e^4}{\alpha^2}\right]^{3/2}} 2\theta_e d\theta_e. \quad (38)$$

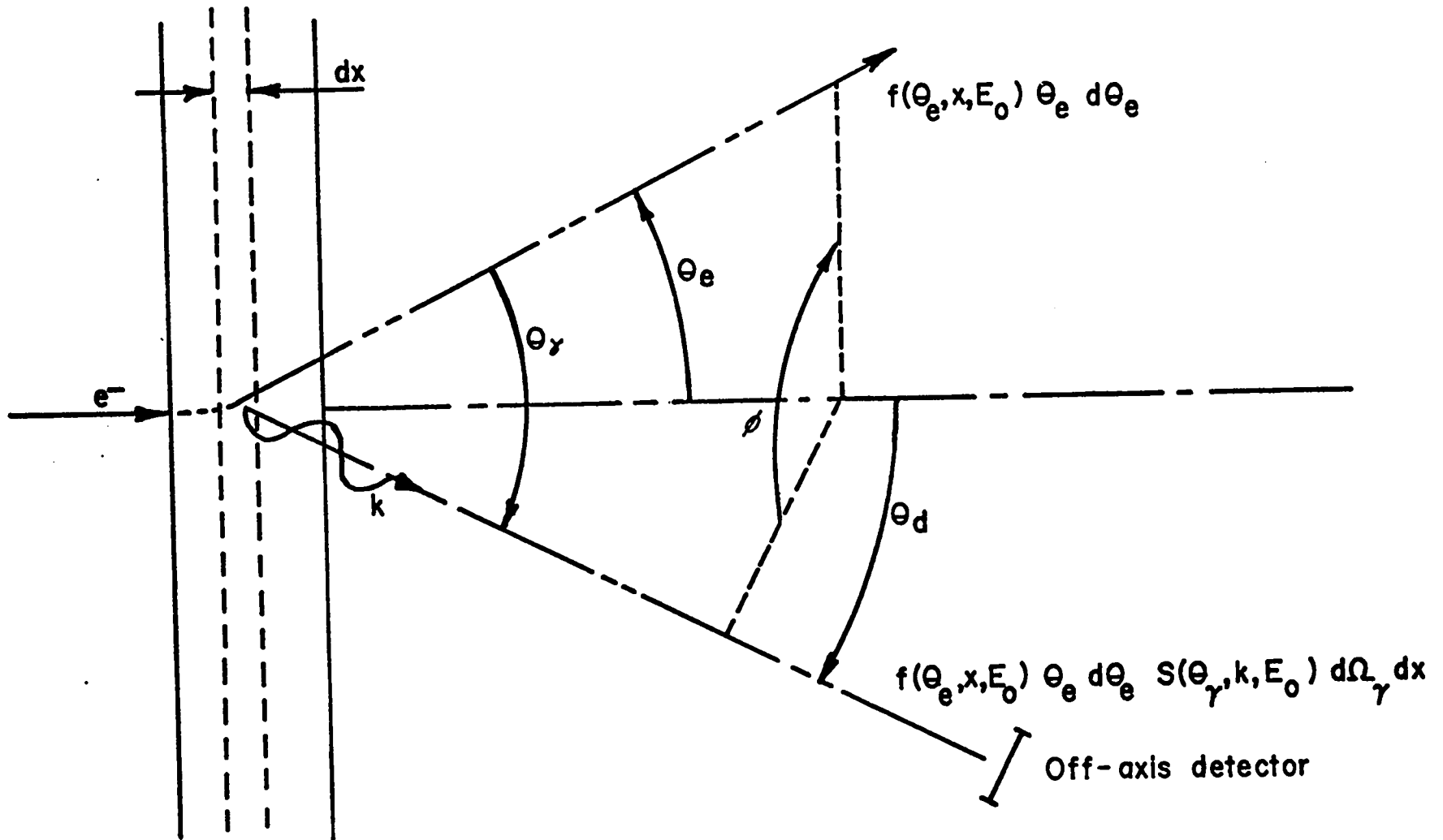


Fig. 5 Thick target geometry.

For convenience, let

$$p' = \alpha p, \quad \frac{\theta^2}{\alpha} = \omega, \quad \frac{\theta^2}{\alpha(1+\omega)} = \delta, \quad \text{then } 2\theta_e d\theta_e = \alpha(1+\omega)d\delta, \quad (39)$$

and the weighting function becomes

$$W(x, E_0, \omega) = \frac{1}{(1+\omega)^2} \int_{\delta=0}^{\infty} \frac{1+\delta}{\left[1 + \frac{2(1-\omega)}{1+\omega} \delta + \delta^2\right]^{3/2}} p'(1+\omega) \exp\{-p'(1+\omega)\delta\} d\delta. \quad (40)$$

This equation is not analytically integrable except for  $\omega = 0$ . However, an accurate approximation can be obtained. By rearranging the terms of Eq. (40),

$$W(x, E_0, \omega) = \frac{1}{(1+\omega)^2} \int_{\delta=0}^{\infty} \left[ \frac{1}{(1+\delta)^2} + \left\{ \frac{1+\delta}{\left[1 + \frac{2(1-\omega)}{1+\omega} \delta + \delta^2\right]^{3/2}} - \frac{1}{(1+\delta)^2} \right\} \right] p'(1+\omega) \exp\{-p'(1+\omega)\delta\} d\delta. \quad (41)$$

A close inspection of the factor,

$$\left\{ \frac{1+\delta}{\left[1 + \frac{2(1-\omega)}{1+\omega} \delta + \delta^2\right]^{3/2}} - \frac{1}{(1+\delta)^2} \right\},$$

shows that it is a resonant type, where the resonance occurs for  $\delta = 1$ . The larger the  $\omega$ , the sharper and higher is the resonance. The integration over this resonance can be performed accurately if the integrand is accurately expressed in the region of resonance, and only approximately expressed elsewhere. Thus, we can rewrite our integral as

$$\begin{aligned}
 W(x, E_0, \omega) = & \frac{1}{(1+\omega)^2} \int_{\delta=0}^{\infty} \frac{1}{(1+\delta)^2} p'(1+\omega) \exp\{-p'(1+\omega)\delta\} d\delta \\
 & + \frac{1}{(1+\omega)^2} \int_{\delta=0}^{\infty} \left[ \frac{1+\delta}{\left[1 + \frac{2(1-\omega)}{1+\omega} \delta + \delta^2\right]^{3/2}} - \frac{1}{(1+\delta)^2} \right] p'(1+\omega) \\
 & \exp\{-p'(1+\omega)\} \exp\{-p'(1+\omega)(\delta-1)\} d\delta .
 \end{aligned} \tag{42}$$

The term,  $\exp\{-p'(1+\omega)(\delta-1)\}$ , can be approximated several ways in the region near  $\delta = 1$ .

Approximation a

$$\exp\{-p'(1+\omega)(\delta-1)\} = 1.$$

Approximation b

(43)

$$\exp\{-p'(1+\omega)(\delta-1)\} = 1 + \frac{2(1-\delta)}{1+\delta} p'(1+\omega).$$

The second approximation is more accurate in the region  $\delta = 1$  because both the value and the derivative match. However, either approximation will produce the same integrated result. Therefore, using either approximation, Eq. (42) can be integrated and yields

$$W(x, E_0, \omega) = \frac{1}{(1+\omega)^2} \left\{ p'(1+\omega) + \int_0^1 p'(1+\omega) e^{p'(1+\omega)} E_1(-p'(1+\omega)) + \omega p'(1+\omega) e^{-p'(1+\omega)} \right\}. \quad (44)$$

This equation reduces to Eq. (18) for  $\omega = 0$ . Here  $W(x, E_0, \omega)$  can be interpreted as the weighting function for the production of detected bremsstrahlung at the depth  $x$  of the target per unit solid angle of the detector, where the detector is oriented at an angle of  $\theta_d$  off-axis.

Figure 6 shows three graphs of the weighting function for values of  $\omega_0 = E_0^2 \theta_d^2$  of 0, 1.0, and 4.0. In contrast to the on-axis bremsstrahlung ( $\omega_0 = 0$ ), where the bremsstrahlung is generated in the leading edge of the target, the off-axis bremsstrahlung is generated at a deeper level. The effect seen in Fig. 6 of the resonant term for  $\omega_0 = 1$  and  $\omega_0 = 4$  shows the peak generation becoming deeper as the observation angle increases. The physical significance of this resonance term can be explained intuitively. For a given angular displacement of the detector, a very thin target will produce a response given only by the angular bremsstrahlung distribution. As the thickness is increased, the electron scattering becomes greater, and a greater proportion of the more abundant forward-generated bremsstrahlung (forward with respect to the scattered electrons) will reach the detector. As the thickness is further increased, a distribution equilibrium is established and the detected intensity falls off monotonically. This effect can be more easily visualized by reorganizing the terms of Eq. (44).

$$W(x, E_0, \omega) = \frac{1}{1+\omega} \left\{ p'(1+\omega) + \int_0^1 p'(1+\omega) e^{p'(1+\omega)} E_1(-p'(1+\omega)) \right\} + \frac{\omega}{(1+\omega)^2} \left\{ p'(1+\omega) e^{-p'(1+\omega)} - p'(1+\omega) - \int_0^1 p'(1+\omega) e^{p'(1+\omega)} E_1(-p'(1+\omega)) \right\}. \quad (45)$$

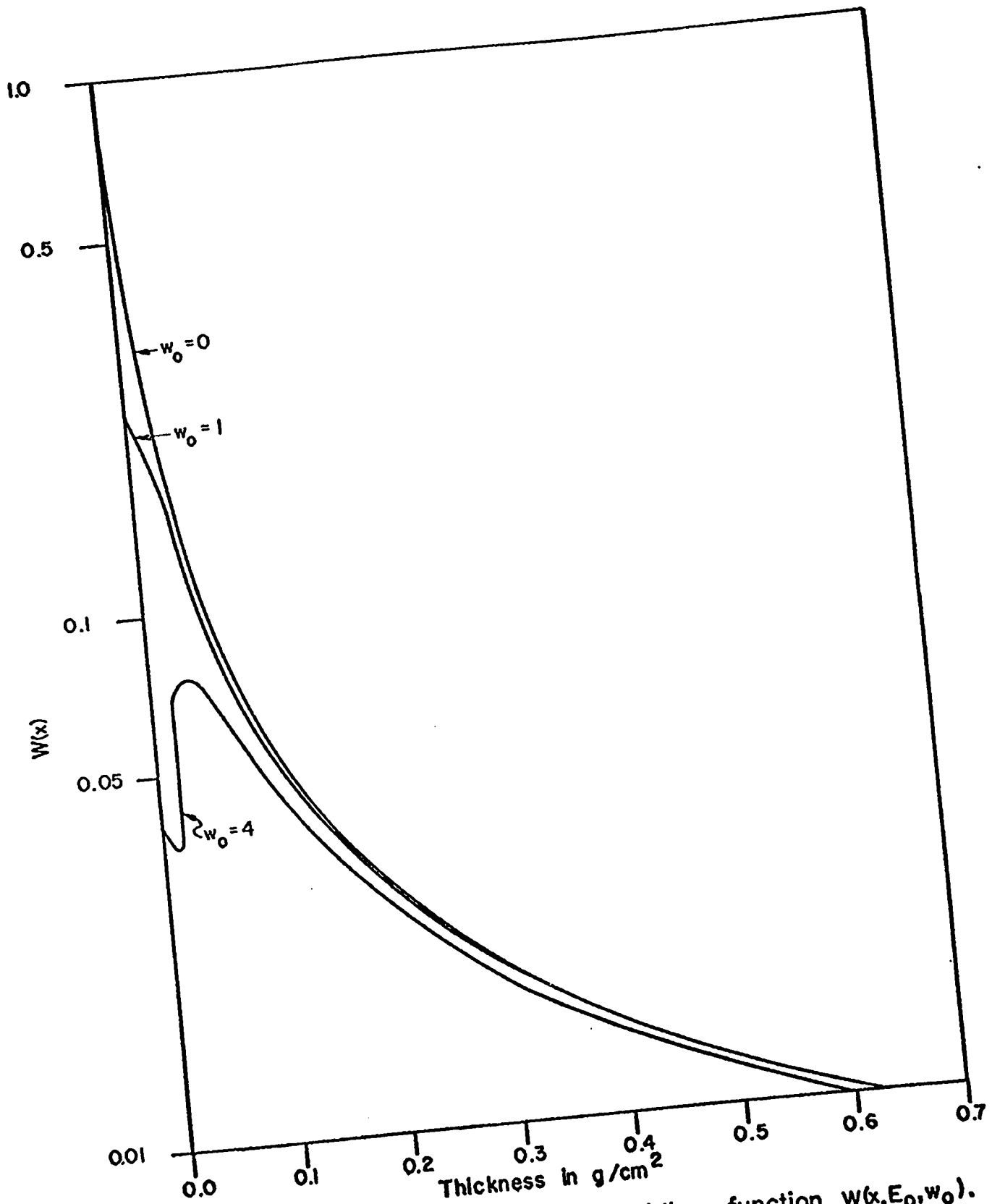


Fig. 6. Bremsstrahlung weighting function  $W(x, E_0, w_0)$ .

The first term is a monotonically decreasing function for  $x$  increasing, while the second term has a resonant characteristic, then falls off much faster than the first term.

### C. The Weighting Function - An Approximation

Equation (45) is a complicated function of the thickness  $x$ . However, as shown in Chap. I, a simple, accurate approximation ( $\sim 3\%$ ) can be made that will lead to integrable results. At first inspection, it seems coincidental that such an approximation can be made; however, a similar result would have appeared at this stage if a reasonable Gaussian approximation to the bremsstrahlung angular distribution had been made early in the theoretical development.<sup>8</sup> Waiting until later to make the approximation revealed how accurate the approximation really was.

The term

$$p'(1+\omega) + \left[ p'(1+\omega) \right]^2 e^{p'(1+\omega)} E_1(-p'(1+\omega)) \quad (46)$$

can be rewritten in the following form

$$\left\{ \left[ \frac{l}{l+l^2 e^l E_1(-l)} - l \right] \frac{1}{l} \frac{1+\omega}{x} \right\} \frac{x}{1+\omega} + 1, \quad (47)$$

where

$$l = \left[ p'(1+\omega) \right]$$

in the nomenclature of Chap. I. The term enclosed by the brackets in Eq. (47) is a slowly varying function of  $x$  in the region where  $x$  contributes significantly to the  $x$  integration. Thus,

$$W_1(x, E_0, \omega) \approx \frac{1}{1+\omega} \left[ 1 + \frac{\bar{a} x}{1+\omega} \right]^{-1}, \quad (48)$$

where  $\bar{a}$  is an average value. It is also interesting to note that  $\omega$  is  $x$ -dependent,  $\omega = \omega_0 \exp\{-2\xi x\}$ ; however, as  $\xi \ll \bar{a}$ , for any value of  $x$  which is large enough to cause a significant change in  $\omega$ , the  $\omega$ -dependence of  $W_1$  will disappear. Thus,

$$W_1(x, E_0, \omega_0) = \frac{1}{1+\omega_0} \left[ 1 + \frac{\bar{a} x}{1+\omega_0} \right]^{-1}. \quad (49)$$

Using the same type of arguments stated above, the second term of Eq. (45) becomes

$$W_2(x, E_0, \omega_0) = \frac{\omega_0}{(1+\omega_0)^2} \left\{ \frac{1+\omega_0}{\bar{a}x} e^{-\left(\frac{1+\omega_0}{\bar{a}x}\right)} - \left(1 + \frac{\bar{a}x}{1+\omega_0}\right)^{-1} \right\}. \quad (50)$$

#### D. Thick Target Bremsstrahlung

Having developed the weighting function into an integrable form, the intensity at the displaced detector, by analogy to the development generated in Chap. I, becomes

$$dI(k, t) = \frac{nNk}{\rho} S_1(k, E_0) e^{-\mu(k)t} \int_0^{t'} \left[ \frac{1}{1+\omega_0} \left\{ \frac{1}{1 + \frac{\bar{a}x}{1+\omega_0}} \right\} + \frac{\omega_0}{(1+\omega_0)^2} \left\{ \frac{1+\omega_0}{\bar{a}x} e^{-\left(\frac{1+\omega_0}{\bar{a}x}\right)} - \frac{1}{1 + \frac{\bar{a}x}{1+\omega_0}} \right\} \right] e^{-Dx} dx dk. \quad (51)$$

Both terms decrease rapidly when increasing  $x$ . Again, as  $D \ll \bar{a}$ , the integration for the second term is essentially complete before  $e^{-Dx}$  deviates from unity. With little loss in accuracy,

$$dI(k,t) = \frac{nNk}{\rho} S_1(k, E_0) e^{-\mu(k)t} \int_0^{t'} \left[ \frac{1}{1+\omega_0} \left\{ \frac{1}{1 + \frac{\bar{a}x}{1+\omega_0}} \right\} e^{-Dx} + \frac{\omega_0}{(1+\omega_0)^2} \right. \\ \left. \left\{ \frac{1+\omega_0}{\bar{a}x} e^{-\left(\frac{1+\omega_0}{\bar{a}x}\right)} - \frac{1}{1 + \frac{\bar{a}x}{1+\omega_0}} \right\} \right] dx dk. \quad (52)$$

Equation (52) can now be integrated directly, and leads to

$$dI(k,t) = \frac{nNk}{\rho} S_1(k, E_0) e^{-\mu(k)t} \left[ \frac{1}{\bar{a}} e^{D(1+\omega_0)/\bar{a}} \left\{ E_i \left[ - \left( \frac{1+\omega_0}{\bar{a}} + t' \right) D \right] \right. \right. \\ \left. \left. - E_i \left[ - \frac{1+\omega_0}{\bar{a}} D \right] \right\} + \frac{\omega_0}{\bar{a}(1+\omega_0)} \left\{ -E_i \left[ - \frac{1+\omega_0}{\bar{a}t'} \right] - \ln \left( 1 + \frac{\bar{a}t'}{1+\omega_0} \right) \right\} \right] dk. \quad (53)$$

The exponential integrals in the first term can be accurately approximated according to the development in Appendix D, then

$$dI(k,t) = \frac{nNk}{\bar{a} \rho} S_1(k, E_0) e^{-\mu(k)t} \left[ \left\{ \ln \left( 1 + \frac{\bar{a}t'}{1+\omega_0} \right) - 2 \ln(1 + Dt'/2) \right. \right. \\ \left. \left. - \frac{\omega_0}{1+\omega_0} C \right\} + \frac{\omega_0}{1+\omega_0} \left\{ C - \ln \left( 1 + \frac{\bar{a}t'}{1+\omega_0} \right) - E_i \left( - \frac{1+\omega_0}{\bar{a}t'} \right) \right\} \right] dk \quad (54)$$

where  $C$  is Euler's constant. This development is based on the assumption that either  $(1+\omega_0)/\bar{a} \ll t'$  or  $Dt' \ll 1$ , a condition that is always met in the practical case. The second term is a correction that is negligible for  $(1+\omega_0)/\bar{a}t' \ll 1$ ; thus it needs only to be evaluated for photon energies approaching the energy of the incident electron energy or for very thin targets.

#### E. Optimum Target Thickness

Equation (54) reveals that the optimum target thickness will be dependent upon the detector's angular position. Consider the practical

use of electron accelerators to radiograph high-Z materials. The target will be tungsten or gold, and the absorption cross section for the object will have a minimum of about 3.5 MeV. It is desirable to calculate the target thickness that will give the maximum detected intensity for a given angular position of the detector. The optimum thickness can be calculated by using Eq. (C-2), Appendix C. Table I lists the various pertinent parameters and the results for gold and tungsten for electron energy of 25 MeV.

Fortunately, the detected intensity near optimum target thickness is extremely flat and the optimum thickness can be taken anywhere between 2 and 3 g/cm<sup>2</sup> for either tungsten or gold targets with the assurance that the intensity for any angular position of the detector will be within a few percent of its maximum value. The target thickness can be designated as 2.42 g/cm<sup>2</sup>, which is equivalent to 0.129 cm (about 50 mils).

The calculations for optimum thicknesses are not particularly good because the maximum intensity is very sensitive to the approximation made for  $W(x, \omega_0)$ , especially for large values of  $x$  near the optimum. However, because of the extreme flatness near the peak, this deficiency is not particularly important and any value of  $x$  near the calculated optimum will give the optimum response. Various factors that are ignored in this theory could easily influence the optimum thickness calculations; for example, the increased distance traveled by the electrons due to scattering prior to their emergence from the target. However, this effect, and probably others not included in this discussion, will not affect the spectral distribution or the angular dependence to any practical degree (probably less than a few percent). Therefore, no attempt is made to increase the accuracy of the optimum thickness determination.

TABLE I  
OPTIMUM TARGETS

Target	$E_0$ (MeV)	$\mu(k)$ ( $\text{cm}^2/\text{g}$ )	$\xi$ ( $\text{cm}^2/\text{g}$ )	$\Delta$ ( $\text{cm}^2/\text{g}$ )	$D$ ( $\text{cm}^2/\text{g}$ )
W (Z=74)	25	0.041	0.195	-0.026	0.375
Au (Z=79)	25	0.042	0.203	-0.027	0.391

Detector Position $\omega_0 = E_0^2 \theta_d^2$	Optimum Thickness ( $\text{g}/\text{cm}^2$ )	
	W	Au
0	2.06	1.99
1	2.25	2.18
4	2.51	2.43
9	2.72	2.62
16	2.90	2.79
25	3.06	2.97

#### F. Angular Intensity Distribution for Optimum Target

Equation (54) shows that the only factor affecting the relative angular distribution is

$$\left\{ \ln\left(1 + \frac{\bar{a}t'}{1+\omega_0}\right) - 2\ln\left(1 + \frac{Dt'}{2}\right) - \frac{\omega_0}{1+\omega_0} \right\} \frac{1}{\bar{a}} . \quad (55)$$

This function can be evaluated for gamma rays of energy  $k = 3.49$  MeV and thickness  $t = t' = 2.42$  g/cm<sup>2</sup>. Because the only term which is a function of  $k$  is  $D(k)$  and its effect is quite small for small angles, the distribution in the approximation is fairly independent of  $k$ . Figure 7 shows this angular distribution evaluated for optimum thickness of target, for values of  $\bar{a}$  given in Appendix F, and for the value of  $D$  given in Table I. The relative distribution for a differentially thin target is also plotted for comparison.

#### G. Variation of the Spectral Distribution with Angle

Because the parameter  $D = 2\xi(k) - \mu(k) - \Delta(k)$  is energy dependent, there is a small variation of the spectral distribution with a change in  $\omega_0$ , the angular position of the detector. This variation is greatest at the high-energy end of the spectrum. Figure 8 shows the spectral distribution for  $\omega_0 = 0$  and for  $\omega_0 = 9$ , the approximate half-intensity angle, for an optimum thickness target. For a better comparison, each curve has been divided by  $\ln\left\{1 + \bar{a}t/(1 + \omega_0)\right\} - \omega_0/(1 + \omega_0)$ . The two curves have a nearly constant difference, thus making the percentage change at the high energy end considerably larger.

#### H. Summary

Although many theories have been presented in the literature (Refs. 4, 5, 6, 8, 9), all have a range of validity, and the assumptions are not

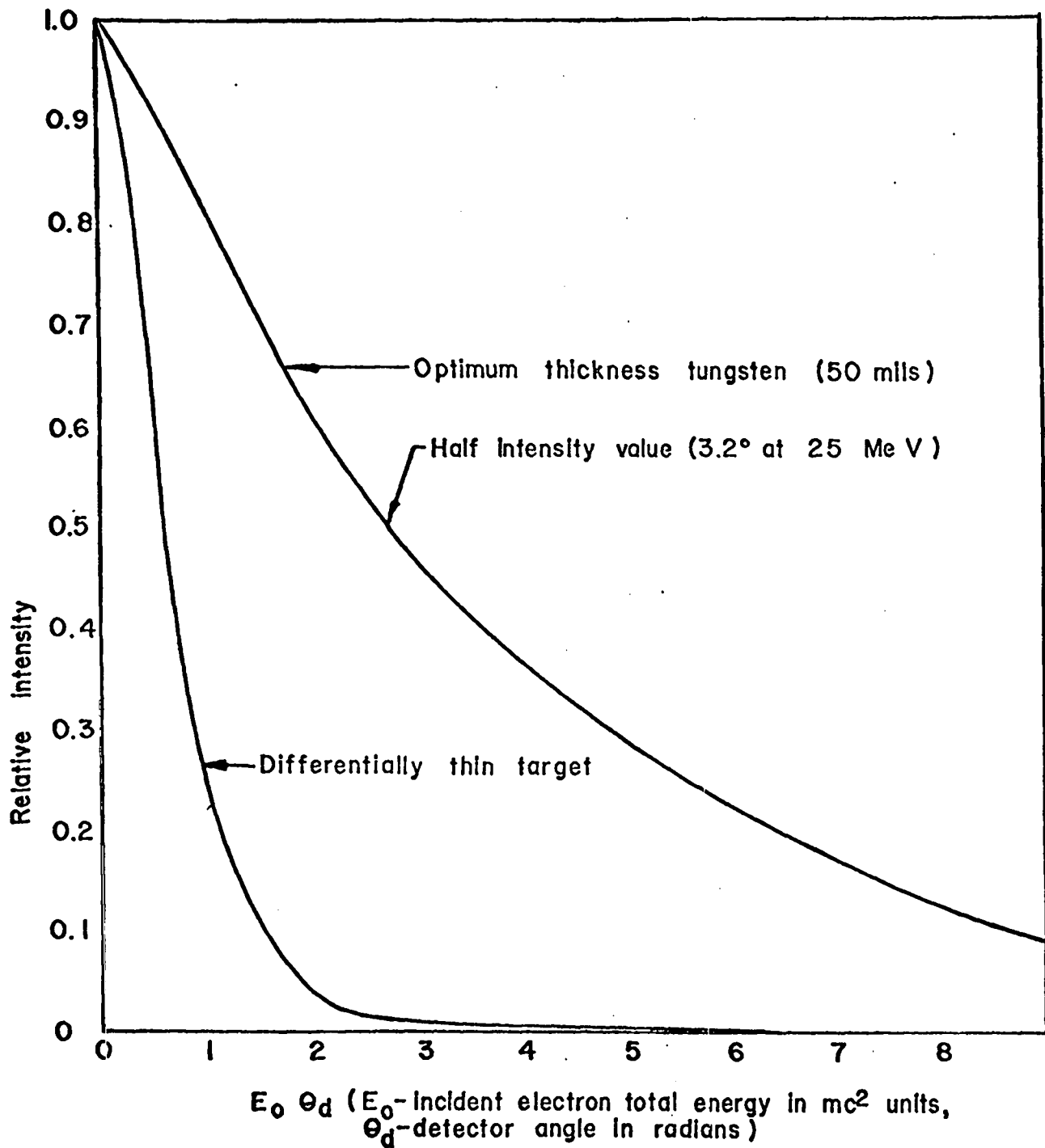


Fig. 7. Bremsstrahlung angular distribution for 3.5-MeV photons.

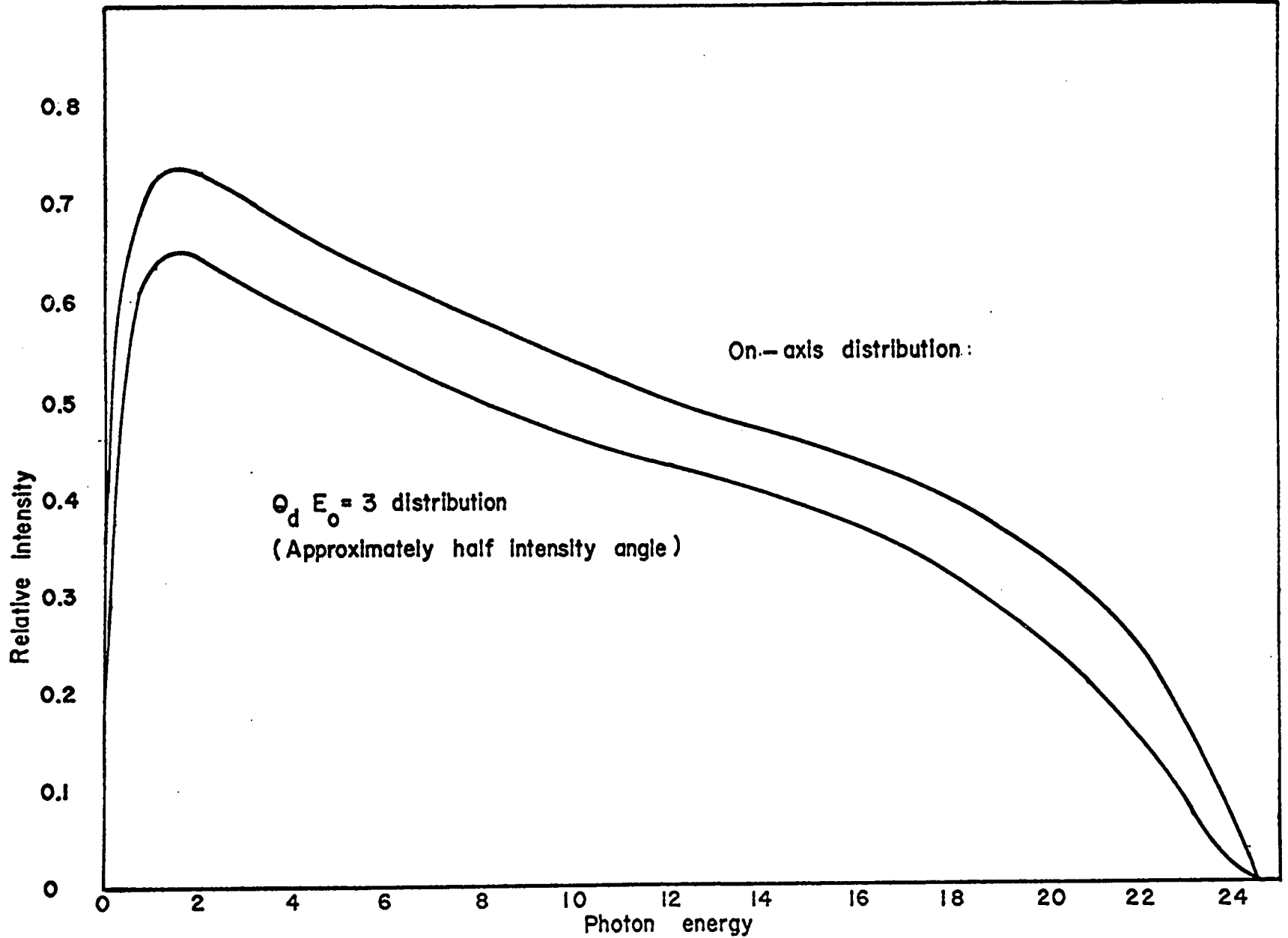


Fig. 8. 25-MeV bremsstrahlung distributions. Each curve is normalized by dividing by  $\left[ \ln \left( 1 + \frac{at}{1+w_0} \right) - \frac{w_0}{1+w_0} \gamma \right]$ .

all-inclusive regarding parameters now considered important in determining the useful detail of the bremsstrahlung angular and spectral distributions. The theory presented here has a range of validity for target thickness from zero to infinity, and for angular position from zero to angles larger than the half-intensity angle. The final equation is

$$dI(k,t) = \frac{nNk}{\bar{a} \rho} S_1(k, E_0) e^{-\mu(k)t} \left[ \left\{ \ln\left(1 + \frac{\bar{a}t'}{1+\omega_0}\right) - 2\ln\left(1 + \frac{Dt'}{2}\right) - \frac{\omega_0}{1+\omega_0} c \right\} + \frac{\omega_0}{1+\omega_0} \left\{ -E_1\left(-\frac{1+\omega_0}{\bar{a}t'}\right) - \ln\left(1 + \frac{\bar{a}t'}{1+\omega_0}\right) + c \right\} \right]. \quad (56)$$

Although the formula looks rather complicated, the second term is small except when  $(1 + \omega_0) \gg \bar{a}t'$ . This occurs only at large angles, when  $k$  is close to its maximum value  $\mathcal{E}_0$ , or when  $t'$  becomes small. The conditions for the validity of the first term is that  $(1 + \omega_0) \ll \bar{a}t'$  or  $(1/2)Dt', \ll 1$ , a condition that is always met in the practical case.

The leading term in this expression is

$$dI(k,t) \sim S_1(k, E_0) e^{-\mu(k)t} \ln\left(1 + \frac{\bar{a}t'}{1+\omega_0}\right), \quad (57)$$

and can be compared with results obtained by others. The main differences in this expression are the new parameter  $t'$ , which has been introduced to replace  $t$ , and the angular dependence  $(1 + \omega_0)$ . Chapter III compares these theoretical results with those previously obtained by others.

CHAPTER III

IMPROVEMENTS IN DEVELOPMENT OF OFF-AXIS BREMSSTRAHLUNG THEORY

A. Improved Approximations

1. The Weighting Function.

In Chap. II only the first term of Molière's theory for electron scattering was considered. In some cases, however, experimental results have been obtained in the region of large angles where multiple scattering might play a lesser role, and plural scattering could account for most of the electron intensity. Examining this effect on the angular radiation distribution for a finite thick target, more accurate Born-approximation corrections have been applied to Molière's theory by Nigam, Sundaresan, and Wu.<sup>10</sup>

Rewriting Eq. (40), using the corrected Molière's theory as it applies to relativistic electrons, the results are

$$W = \frac{\ell}{(1+\omega)^2} \int_{\delta=0}^{\infty} \frac{(1+\delta)d\delta}{\left(1 + \frac{2(1-\omega)}{(1+\omega)} \delta + \delta^2\right)^{\frac{3}{2}}} \int_{y=0}^{\infty} J_0(2y^{\frac{1}{2}} \ell^{\frac{1}{2}} \delta^{\frac{1}{2}}) e^{-y} \left[ 1 + \frac{y}{B} \ln y - \frac{2\pi\alpha}{B_p^{\frac{1}{2}} E_x} y^{\frac{1}{2}} + \text{higher order terms} \right] dy. \quad (58)$$

Not being satisfied that the various terms in Eq. (58) are analytically nonintegrable, many attempts have been made to solve them exactly. These attempts have failed. However, in the mathematical exploration, an approximate derivation has been found that gives results similar to Eq. (37) and which agree more closely with the experimental data. This convincing derivation follows. Consider only the  $\delta$  intergral of Eq. (58)

$$\int_{\delta=0}^{\infty} \frac{(1+\delta)}{\left(1 + 2 \frac{(1-\omega)}{(1+\omega)} \delta + \delta^2\right)^{\frac{3}{2}}} J_0(2y^{\frac{1}{2}} \rho^{\frac{1}{2}} \delta^{\frac{1}{2}}) d\delta \quad (59)$$

and let  $\delta^{\frac{1}{2}} = \Sigma$ ,  $L = 2y^{\frac{1}{2}} \rho^{\frac{1}{2}}$ ,  $A^2 = (1-\omega)/(1+\omega)$  for  $\omega \leq 1$ , and  $A^2 = (\omega-1)/(\omega+1)$  for  $\omega \geq 1$ .

Making these substitutions, the integral becomes

$$\lim_{b \rightarrow 1} \frac{2}{L^{\frac{3}{2}}} \int_{\Sigma=0}^{\infty} \frac{(1+\Sigma^2) \Sigma^{\frac{1}{2}}}{\left(b^4 \pm 2A^2 \Sigma^2 + \Sigma^4\right)^{\frac{3}{2}}} J_0(L\Sigma)(L\Sigma)^{\frac{1}{2}} d\Sigma, \quad (60)$$

where b is introduced as a free parameter.

Because

$$-\frac{1}{2b^3} \frac{d}{db} (b^4 \pm 2A^2 \Sigma^2 + \Sigma^4)^{-\frac{1}{2}} = (b^4 \pm 2A^2 \Sigma^2 + \Sigma^4)^{-\frac{3}{2}}$$

and

$$\pm \frac{1}{2A} \frac{d}{dA} (b^4 \pm 2A^2 \Sigma^2 + \Sigma^4)^{-\frac{1}{2}} = \Sigma^2 (b^4 \pm 2A^2 \Sigma^2 + \Sigma^4)^{-\frac{3}{2}},$$

Equation (60) can be rewritten as

$$\lim_{b \rightarrow 1} -\frac{1}{L^{\frac{3}{2}}} \left( \pm \frac{1}{A} \frac{d}{dA} + \frac{1}{b^3} \frac{d}{db} \right) \int_{\Sigma=0}^{\infty} \Sigma^{\frac{1}{2}} (b^4 \pm 2A^2 \Sigma^2 + \Sigma^4)^{-\frac{1}{2}} J_0(L\Sigma)(L\Sigma)^{\frac{1}{2}} d\Sigma. \quad (61)$$

This can be directly integrated using Hankel<sup>11</sup> transforms

$$\lim_{b \rightarrow 1} \left( \pm \frac{1}{A} \frac{d}{dA} - \frac{1}{b^3} \frac{d}{db} \right) K_0 \left\{ \left( \frac{1}{2} b^2 \pm \frac{1}{2} A^2 \right)^{\frac{1}{2}} L \right\} J_0 \left\{ \left( \frac{1}{2} b^2 \mp \frac{1}{2} A^2 \right)^{\frac{1}{2}} L \right\}. \quad (62)$$

Carrying out the indicated differentiations, collecting like terms,

letting  $b \rightarrow 1$ , and substituting for  $A^2$  and  $L$ , the integral becomes

$$(1+\omega) J_0 \left( 2\omega^{\frac{1}{2}} p^{\frac{1}{2}} y^{\frac{1}{2}} \right) K_1 \left( 2p^{\frac{1}{2}} y^{\frac{1}{2}} \right) 2p^{\frac{1}{2}} y^{\frac{1}{2}}. \quad (63)$$

Substituting Eq. (63) back into the expression for the weighting function,

Eq. (58) then becomes

$$W = \int_{y=0}^{\infty} p J_0\left(2\omega^{\frac{1}{2}} p^{\frac{1}{2}} y^{\frac{1}{2}}\right) K_1\left(2p^{\frac{1}{2}} y^{\frac{1}{2}}\right) 2p^{\frac{1}{2}} y^{\frac{1}{2}} e^{-y} \left[1 + \frac{y}{B} \ln y - \frac{2\pi\alpha}{B^{\frac{1}{2}} E_x} y^{\frac{1}{2}} + \text{higher orders of } \frac{y}{B}\right] dy. \quad (64)$$

This expression for the weighting function represents the convolution of the electron-scattering angular distribution and the bremsstrahlung angular distribution as a function of the thickness ( $\sim 1/p$ ). This expression has not been analytically solved; however, the various terms have been evaluated by computer, and the terms in the various powers of  $1/B$  contribute only a few percent to the weighting function for small angles less than  $10^\circ$ . These small contributions will be ignored in the light of the approximate nature of the bremsstrahlung distribution for larger angles. The results indicate that the long, angular-distribution tail of the electron scattering contributes only slightly to the angular-distribution tails of the thick target bremsstrahlung.

Thus, the weighting function reduces to

$$W = \int_{y=0}^{\infty} p J_0\left(2\omega^{\frac{1}{2}} p^{\frac{1}{2}} y^{\frac{1}{2}}\right) K_1\left(2p^{\frac{1}{2}} y^{\frac{1}{2}}\right) 2p^{\frac{1}{2}} y^{\frac{1}{2}} e^{-y} dy. \quad (65)$$

## 2. Weighting Function - An Approximation.

Being unable to integrate Eq. (65) analytically, an approximate means of arriving at a simple, accurate solution was used. First, this equation was solved for zero angle ( $\omega = 0$ ), which can be done exactly.

$$W_{\omega=0} = \int_{y=0}^{\infty} p K_1\left(2p^{\frac{1}{2}} y^{\frac{1}{2}}\right) 2p^{\frac{1}{2}} y^{\frac{1}{2}} e^{-y} dy = p + p^2 e^p E_1(-p), \quad (66)$$

where  $E_1(-p)$  is the exponential integral. However, this form is very difficult to manipulate; therefore, to simplify it, the terms are rearranged.

$$W_{\omega=0} = \frac{p}{p + \left\{ \frac{p}{p + p^2 e^p E_1(-p)} - p \right\}} \quad (66a)$$

The term in brackets is a slowly varying function of  $p$ , which varies from 2 for  $p \rightarrow \infty$  to 1 for  $p \rightarrow 0$ . However, as  $W$  is little influenced by the bracketed term for large values of  $p$ , an average value can be chosen with only a small error introduced in the region that will prove important

$$W_{\omega=0} = \frac{p}{p + v}, \quad v = 1.15. \quad (67)$$

A better approximation, which was considered but complicated some of the succeeding mathematical operations, is given here for reference. The error is only a few percent over the entire range of  $p$ .

$$W_{\omega=0} = \frac{p(p+1)}{(p+\kappa)(p+\lambda)} \quad \begin{aligned} \kappa &= (3 + \sqrt{5})/2 \\ \lambda &= (3 - \sqrt{5})/2 \end{aligned} \quad (67a)$$

Next, consider the integral of Eq. (65) in the region where  $p \gg 1$ . This is the region of greatest contribution to the transmitted intensity. The integral is rewritten as

$$W_{p \rightarrow \infty} = \int_{y=0}^{\infty} p J_0 \left( 2\omega^{\frac{1}{2}} p^{\frac{1}{2}} y^{\frac{1}{2}} \right) K_1 \left( 2p_1^{\frac{1}{2}} y^{\frac{1}{2}} \right) 2p_1^{\frac{1}{2}} y^{\frac{1}{2}} dy. \quad (68)$$

Note that  $p_1$  has been substituted for  $p$  to approximate the effect of the term  $e^{-y}$  for the smaller values of  $p$ , and is evaluated in the following development. Equation (68) can be solved exactly and reduces to

$$W_{p \rightarrow \infty} = \frac{p}{p_1} \frac{1}{\left( 1 + \omega \frac{p}{p_1} \right)^2} \quad (69)$$

If one demands that  $W_{p \rightarrow \infty} = W_{\omega=0}$  for  $\omega = 0$ , then  $p_1 = p + v$  and

$$W_{p \rightarrow \infty} = \frac{p(p + \alpha)}{[(1 + \omega)p + v]^2} = \frac{p}{(1 + \omega)p + v} \left[ 1 - \frac{\omega p}{[(1 + \omega)p + v]} \right]. \quad (70)$$

Equation (70) is not a bad approximation for  $p \rightarrow 0$ . This can be seen by letting

$$W_{p \rightarrow 0} = \int_{y=0}^{\infty} p J_0 \left( 2\omega^{\frac{1}{2}} p^{\frac{1}{2}} y^{\frac{1}{2}} \right) e^{-y p_1} dy, \quad (71)$$

where  $p_1$  is now chosen to approximate the effect of the  $K_1 \left( 2p^{\frac{1}{2}} y^{\frac{1}{2}} \right) 2p^{\frac{1}{2}} y^{\frac{1}{2}}$  term for small  $p$ . Or, upon integrating Eq. (71),

$$W_{p \rightarrow 0} = \frac{p}{p_1} e^{-\omega p / p_1}. \quad (72)$$

If one demands that  $W_{p \rightarrow 0} = W_{\omega = 0}$  for  $\omega = 0$ , again  $p_1 = p + v$ , or

$$W_{p \rightarrow 0} = \frac{p}{p + v} e^{-\omega p / (p + v)} = \frac{p}{(1 + \omega)p + v} \left[ 1 - \frac{\omega^2 p^2}{(p + v)^2} + \dots \right]. \quad (73)$$

The second terms of Eqs. (70) and (73) are nearly the same. Because the second term is only a correction to the identical first terms for  $W$ , then consider a new second term which will, in the limits stated, reduce to values indicated in Eqs. (70) and (73). Consider

$$\frac{\omega p}{(1 + \omega)p + v} = \frac{\omega p [(1 + \omega)p + v]}{[(1 + \omega)p + v]^2}, \quad (74)$$

and allow the  $v$  term in the numerator to be zero, then

$$\lim_{p \rightarrow \infty} \frac{\omega(1 + \omega)p^2}{[(1 + \omega)p + v]^2} \rightarrow \frac{\omega}{1 + \omega},$$

and

$$\lim_{\substack{p \rightarrow 0 \\ v = 1 \\ \omega \text{ large}}} \frac{\omega(1+\omega)p^2}{[(1+\omega)p+v]} \rightarrow \frac{(1+\omega)\omega p^2}{v^2} \approx \omega^2 p^2. \quad (75)$$

Thus, the equation for the weighting function can be approximated closely for all values of  $p$ , that is,

$$W \approx \frac{p}{(1+\omega)p+v} \left[ 1 - \frac{\omega(1+\omega)p^2}{[(1+\omega)p+v]^2} \right]. \quad (76)$$

### 3. Relationship of $p$ to the Thickness $x$ .

In order to prepare Eq. (76) for integration over the thickness parameter,  $x$ , one must find the  $x$ -dependence of  $p$ . Drawing from the previous parts of this report,

$$p = \frac{1}{B\theta_1^2} \frac{1}{E_x^2}, \quad (77)$$

where

$$B = \ln\{1.1\zeta^2 \ln 1.4\zeta^2\},$$

$$\zeta^2 = K_2 \left( e^{2\xi x} - 1 \right) / 2\xi,$$

$$K_2 = 2200Z^{\frac{1}{3}}(Z+1)/A,$$

and

$$\theta_1^2 = K_1 \left( e^{2\xi x} - 1 \right) / 2\xi \cdot 2\mu^2 E_0^2,$$

$$K_1 = 0.314Z(Z+1)/A,$$

$$E_x^2 = E_0^2 e^{-2\xi x}.$$

These equations are based on the fact that the electron's energy falls off exponentially in the region of importance. One can further simplify Eq. (77) by assuming an average value for  $B$  because it is a slowly varying

function of  $x$  in the region where  $p$  will have its effect on  $W$ . Also,  $2x \ll 1$  for any practical thickness which contributes to the intensity from a thick target. Making these good approximations yields

$$p = 2\mu^2/K_1 B x e^{-\xi x} = \nu/\bar{a} x e^{-\xi x}. \quad (78)$$

One evaluates  $\bar{a}$  by choosing an approximate value of  $p$  which represents the effective depth of bremsstrahlung. The previous chapters show this to be in the region of  $p = 0.1$ . Using this value for  $p$ ,  $\nu = 1.15$ , assuming  $\xi x \rightarrow 0$  for this depth, and using the relationships shown by Eq. (77),  $\bar{a}$  can be solved.

$$\bar{a} = 11.15 K_2 / \zeta_e^2,$$

where  $\zeta_e^2$  is determined by

$$\zeta_e^2 \ln\{1.1\zeta_e^2 \ln 1.4\zeta_e^2\} = 5.20 K_2 / K_1. \quad (79)$$

Graphs of this function, Appendix F, can be used for solving for  $\bar{a}$  for the particular material used as the target. For example, gold has a value of  $166.9 \text{ cm}^2/\text{g}$ . In contrast to the Chap. II results, this derivation finds  $\bar{a}$  to be independent of  $\omega$ , thus simplifying the results.

#### 4. Thick Target Bremsstrahlung.

Having developed the weighting function into an integrable form, now write the intensity at the angularly displaced detector by analogy to the development generated in the previous parts of this report.

$$dI(k,t) = \frac{nNk}{\rho} S_1(k, E_0) e^{-\mu(k)t} \int_{x=0}^{t'} \left\{ \frac{p}{(1+\omega)p + \nu} - \frac{\omega(1+\omega)p^3}{[(1+\omega)p + \nu]^3} \right\} e^{-Dx} dx dk. \quad (80)$$

Recalling that  $p \approx 1/\bar{a}x$  and that  $\bar{a} \gg 1$ , the integration of the second term is essentially complete before  $\exp(-Dx)$  deviates appreciably from unity. By the same line of reasoning,  $\omega = \omega_0 e^{-2\xi x}$  can be replaced by  $\omega_0$  in the second term; thus, the integral portion of Eq. (80) can be written

$$\int_{x=0}^{t'} \frac{p}{(1+\omega)p + \nu} e^{-Dx} dx + \int_{x=0}^{t'} - \frac{\omega_0 (1 + \omega_0) p^3}{[(1 + \omega_0)p + \nu]^3} dx. \quad (81)$$

Consider the first term and make the substitution  $p = \sqrt{\bar{a}x} e^{-\xi x}$  and again  $\omega = \omega_0 e^{-2\xi x}$ . As  $\xi \ll \bar{a}$ , for any value of  $x$ , which is large enough to cause a significant change in  $\omega$ , the  $\omega$ -dependence of this term will disappear. Thus, the first term can be rewritten with essentially no error

$$\frac{1}{1 + \omega_0} \int_{x=0}^{t'} \left[ 1 + \frac{\bar{a}x}{1 + \omega_0} \right]^{-1} e^{-D'x} dx$$

$$D' = D - \xi = \xi - \mu(k) - \Delta(k). \quad (82)$$

By analogy to the development in the two preceding chapters, the first term becomes

$$\frac{1}{a} \left\{ \ln \left( 1 + \frac{at'}{1 + \omega_0} \right) - 2 \ln \left( 1 + \frac{D't'}{2} \right) \right\} e^{D'(1 + \omega_0)/\bar{a}}. \quad (83)$$

The second term is straightforward and, after integrating, becomes

$$\frac{1}{2a} \left( \frac{\omega_0}{1 + \omega_0} \right) \left[ \frac{1}{\left( 1 + \frac{at'}{1 + \omega_0} \right)} - 1 \right]. \quad (84)$$

The final equation can now be written

$$dI(k,t) = \frac{nNk}{a\rho} S_1(k, E_0) e^{-\mu(k)t}$$

$$\left\{ \left[ \ln\left(1 + \frac{\bar{a}t'}{1 + \omega_0}\right) - 2\ln\left(1 + \frac{D't'}{2}\right) \right] e^{D'(1 + \omega_0)/\bar{a}}$$

$$- \frac{\omega_0}{2(1 + \omega_0)} + \frac{\omega_0}{2(1 + \omega_0)} \left[ \left(1 + \frac{\bar{a}t'}{1 + \omega_0}\right)^{-2} \right] \right\}. \quad (85)$$

This equation is similar to Eq. (54) of Chap. II, except that now  $\bar{a}$  is not  $\omega_0$ -dependent and the final term is simpler and more accurate. It is comforting that the approach used in developing these two equations is completely different, yet, to better than a first order, the results are the same.

## B. Experimental Verification

### 1. Comparisons of Experimental Results.

The comparisons are restricted to the experimental results obtained by Lanzl and Hanson.<sup>8</sup> Their results were obtained from a well-designed experiment using the 20-MeV University of Illinois betatron. The theoretical equation must be corrected for the geometrical arrangement of Lanzl and Hanson.<sup>8</sup>

The most important correction is to compensate for the condition of the beam incident on the target. The theory, as developed in part A of this chapter, was based on an incident beam of parallel rays. In the experiment, the beam from the betatron traversed the thin aluminum walls of a monitor, presenting an incident beam estimated by Lanzl and Hanson<sup>8</sup> to have an  $1/e$  width of  $0.78^\circ$ . The scattering theory incorporates a Gaussian function in Molière's leading term for electron multiple scattering, the incident angular dependence can be approximated by allowing Molière's

Gaussian term to generate this angular spread without allowing Eq. (85) to contribute any bremsstrahlung. This is done by replacing the zero lower limit of Eq. (85) by  $t_i$ , obtained from Molière's Gaussian term,

$$e^{-\theta^2/\theta^2 B_1}, \quad (86)$$

by letting  $\theta^2/\theta^2 B_1 = 1$ , and by using the various relations of Eq. (77) to derive

$$t_i = \zeta_e^2/K_2. \quad (87)$$

The upper limit then becomes  $t' + t_i$  to properly account for the thickness of target traversed by the electrons.

Let Eq. (85) be rewritten in the form

$$dI(k, t, \omega_0) = \frac{nNk}{a\rho} S_1(k, E_0) e^{-\mu(k)t} L(t', \omega_0),$$

where

$$L(t', \omega_0) = \left[ \ln\left(1 + \frac{\bar{a}t'}{1 + \omega_0}\right) - 2\ln\left(1 + \frac{D't'}{2}\right) \right] e^{D'(1 + \omega_0)/\bar{a}} - \frac{\omega_0}{2(1 + \omega_0)} + \frac{\omega_0}{2(1 + \omega_0)} \left(1 + \frac{\bar{a}t'}{1 + \omega_0}\right)^{-2}. \quad (88)$$

Thus, the geometrically corrected differential intensity as a function of photon energy,  $k$ , thickness,  $t$ , angular displacement of the detector,  $\omega_0$ , and the geometrical correction factor,  $t_i$ , becomes

$$dI(k, t, \omega_0)_{\text{corr}} = R(k) \frac{nNk}{a\rho} S_1(k, E_0) e^{-\mu(k)t} \{L(t't_i, \omega_0) - L(t_i, \omega_0)\}. \quad (89)$$

The  $R(k)$  multiplier has been added to account for the spectral response of the detector. Although a correction for the finite entrance aperture

of the detector ( $\sim 0.9^\circ$ ) would slightly ( $< 2\%$ ) improve the results, the complications involved preempted making the calculations. The intensity as seen by the detector becomes

$$I(t, \omega_0) = \int_{k \neq 0}^{k=E_0} R(k) \frac{nNk}{a\rho} S_1(k, E_0) e^{-\mu(k)t} \{L(t' + t_i, \omega_0) - L(t_i, \omega_0)\} dk. \quad (90)$$

It is Eq. (90) that will be compared with the experiment of Lanzl and Hanson as a verification of the correctness of Eq. (85).

## 2. Angular Distribution.

The relative angular distribution can be obtained from Eq. (90).

$$A(t, \omega_0) = \frac{I(t, \omega_0)}{I(t, 0)}. \quad (91)$$

Consider the condition where the thickness  $t < 1 \text{ gm/cm}^2$  for a gold target. Under these conditions,  $t' = t$  for practically all values of  $k$ , making  $L(t' + t_i, \omega_0) - L(t_i, \omega_0)$  essentially independent of  $k$ , thus

$$A(t, \omega_0)_{t < 1} \approx \frac{L(t + t_i, \omega_0) - L(t_i, \omega_0)}{L(t + t_i, 0) - L(t_i, 0)}. \quad (92)$$

Figures 9, 10, and 11 show the angular distribution for gold thicknesses of  $51.5 \text{ mg/cm}^2$ ,  $247.1 \text{ mg/cm}^2$ , and  $967.0 \text{ mg/cm}^2$ , respectively. For the smaller thicknesses, the agreement is remarkably good. Here the theory of Lanzl and Hanson fails for the larger angles, primarily because their two-Gaussian approximation for the bremsstrahlung is not accurate enough. For the thicker target ( $\sim 1 \text{ g/cm}^2$ ), both theories agree with the experimental data.

For the very thick targets, the theory of Lanzl and Hanson does not apply because there is no provision for apparent thickness,  $t'$ , as a function of photon energy,  $k$ . The angular distribution, in this case,

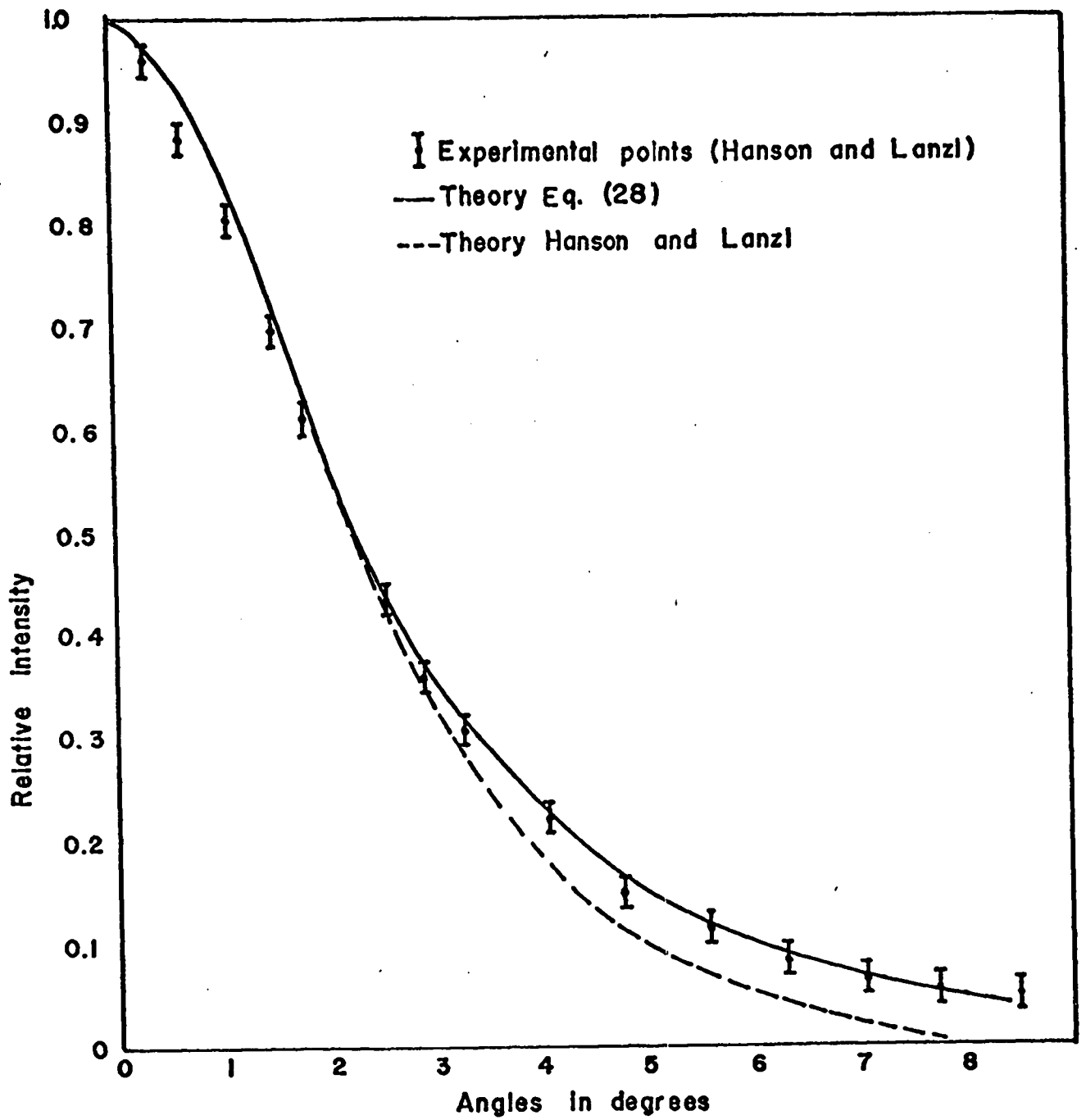


Fig. 9. Angular distribution. Ion chamber detector Au: 51.5 mg/cm<sup>2</sup>.

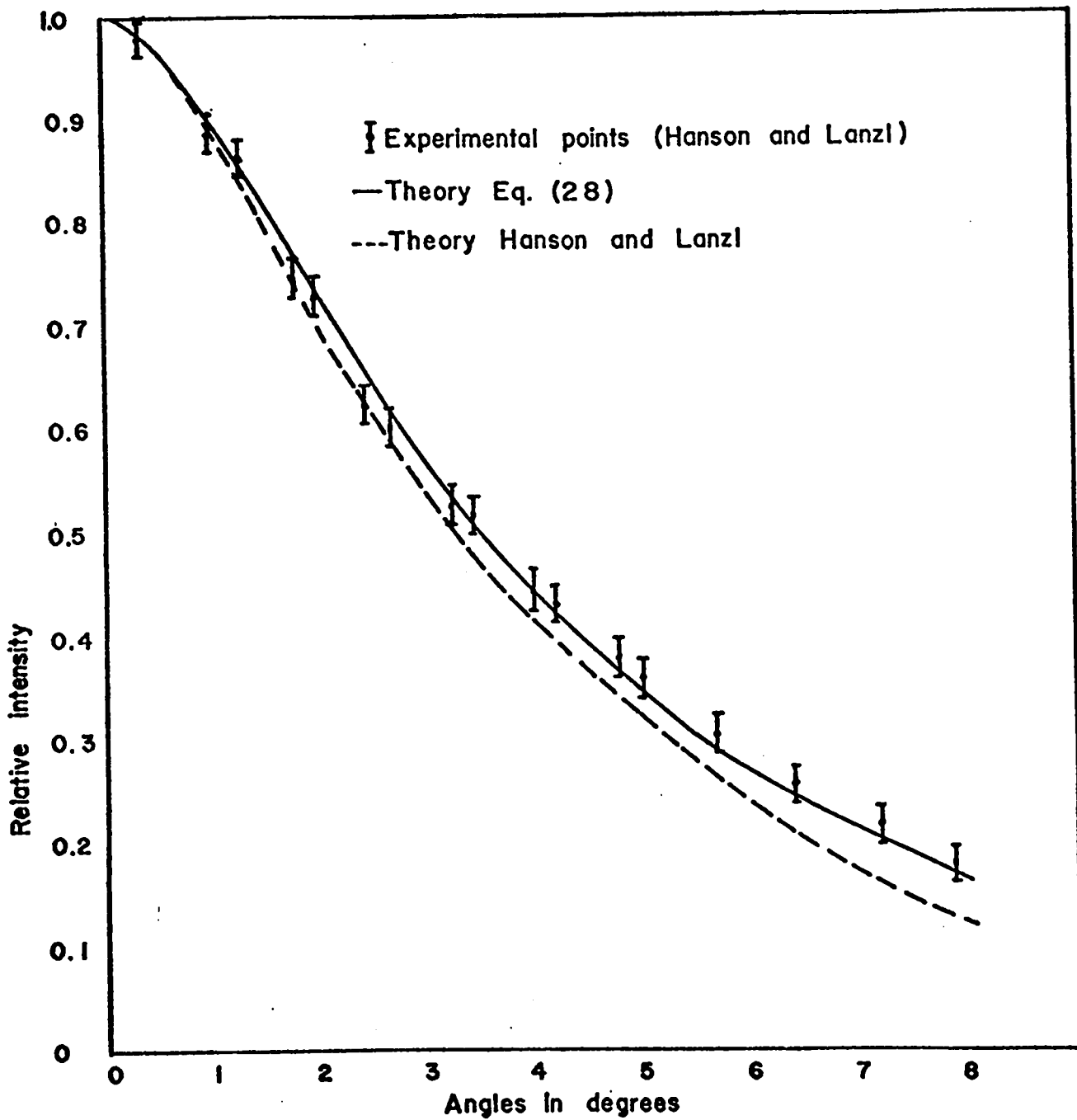


Fig. 10. Angular distribution. Ion chamber detector Au: 247.1 mg/cm<sup>2</sup>.

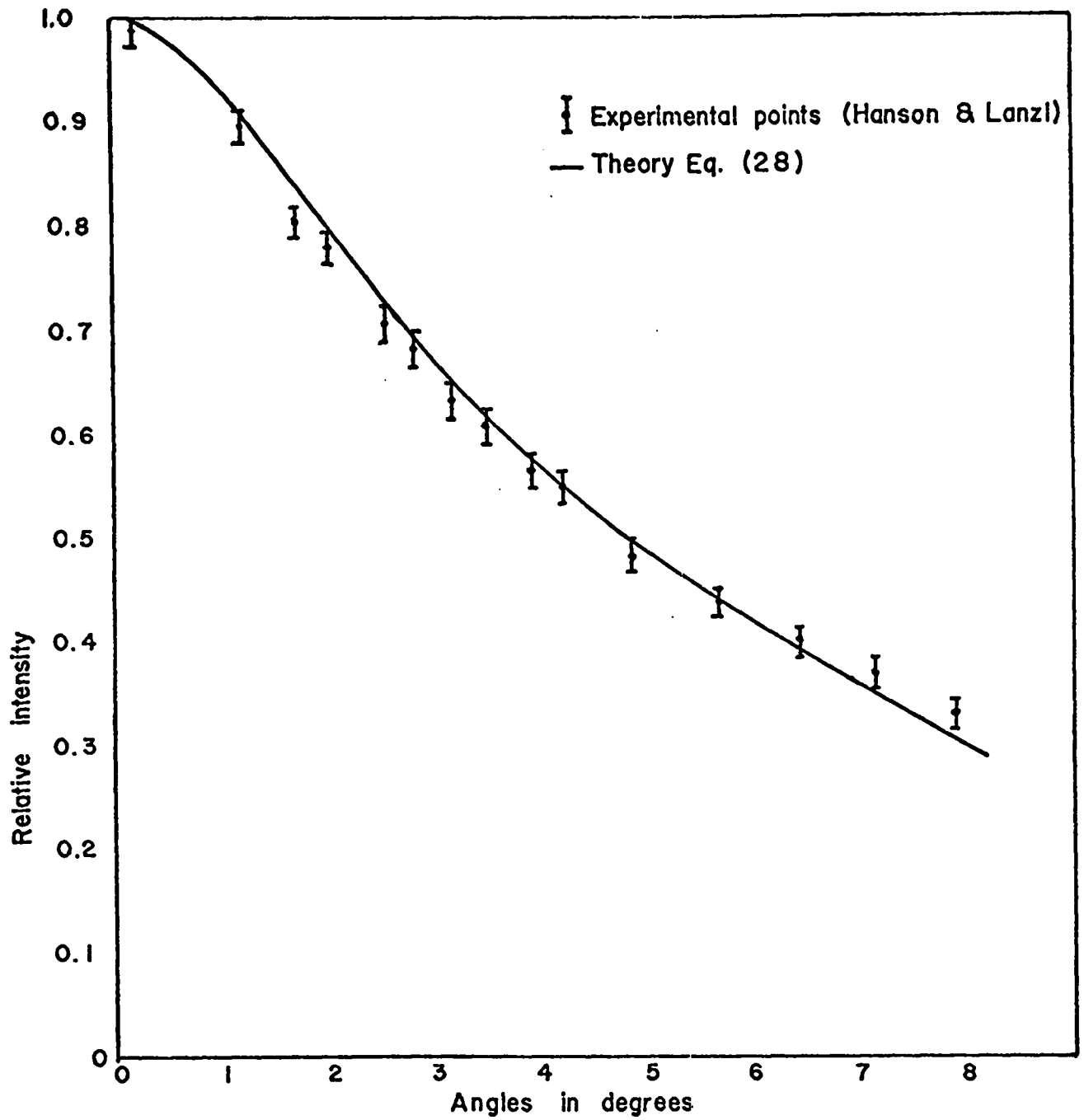


Fig. II. Angular distribution. Ion chamber detector Au. 967.0 mg/cm<sup>2</sup>

can be written

$$A(t, \omega_0)_{t > 1} = \frac{\int_{k=0}^{E_0} R(k) \frac{nNk}{ap} S_1(k, E_0) e^{-\mu(k)t} \{L(t' + t_i, \omega_0) - L(t_i, \omega_0)\} dk}{\int_{k=0}^{E_0} R(k) \frac{nNk}{ap} S_1(k, E_0) e^{-\mu(k)t} \{L(t' + t_i, 0) - L(t_i, 0)\} dk} \quad (93)$$

In order to evaluate this expression, some knowledge of  $R(k)$  is necessary. For the ion detector used, the response is more nearly proportional to the number of quanta rather than the intensity because the ion detector is very thin compared with the mean free path of the secondary electrons involved. Consequently,  $R(k)$  is not a very sensitive parameter, and it is assumed that  $R(k)$  is proportional to  $1/k$ . Thus,

$$A(t, \omega_0) = \frac{\int_{k=0}^{E_0} S_1(k, E_0) e^{-\mu(k)t} \{L(t' + t_i, \omega_0) - L(t_i, \omega_0)\} dk}{\int_{k=0}^{E_0} S_1(k, E_0) e^{-\mu(k)t} \{L(t' + t_i, 0) - L(t_i, 0)\} dk} \quad (94)$$

Figure 12 shows four points calculated by using Eq. (94). The integration indicated was computed graphically for the four points shown, and the experiment and theory agree within experimental error. No comparison could be made with the theory of Lanzl and Hanson since their theory is not valid for this thickness.

### 3. Central Yield.

Another interesting comparison of theory and experiment is the central yield as a function of thickness. Consider Eq. (90), with  $\omega = 0$  and  $R(k) \sim 1/k$

$$I(t, 0) \sim \int_{k=0}^{E_0} S_1(k, E_0) e^{-\mu(k)t} \{L(t' + t_i, 0) - L(t_i, 0)\} dk \quad (95)$$

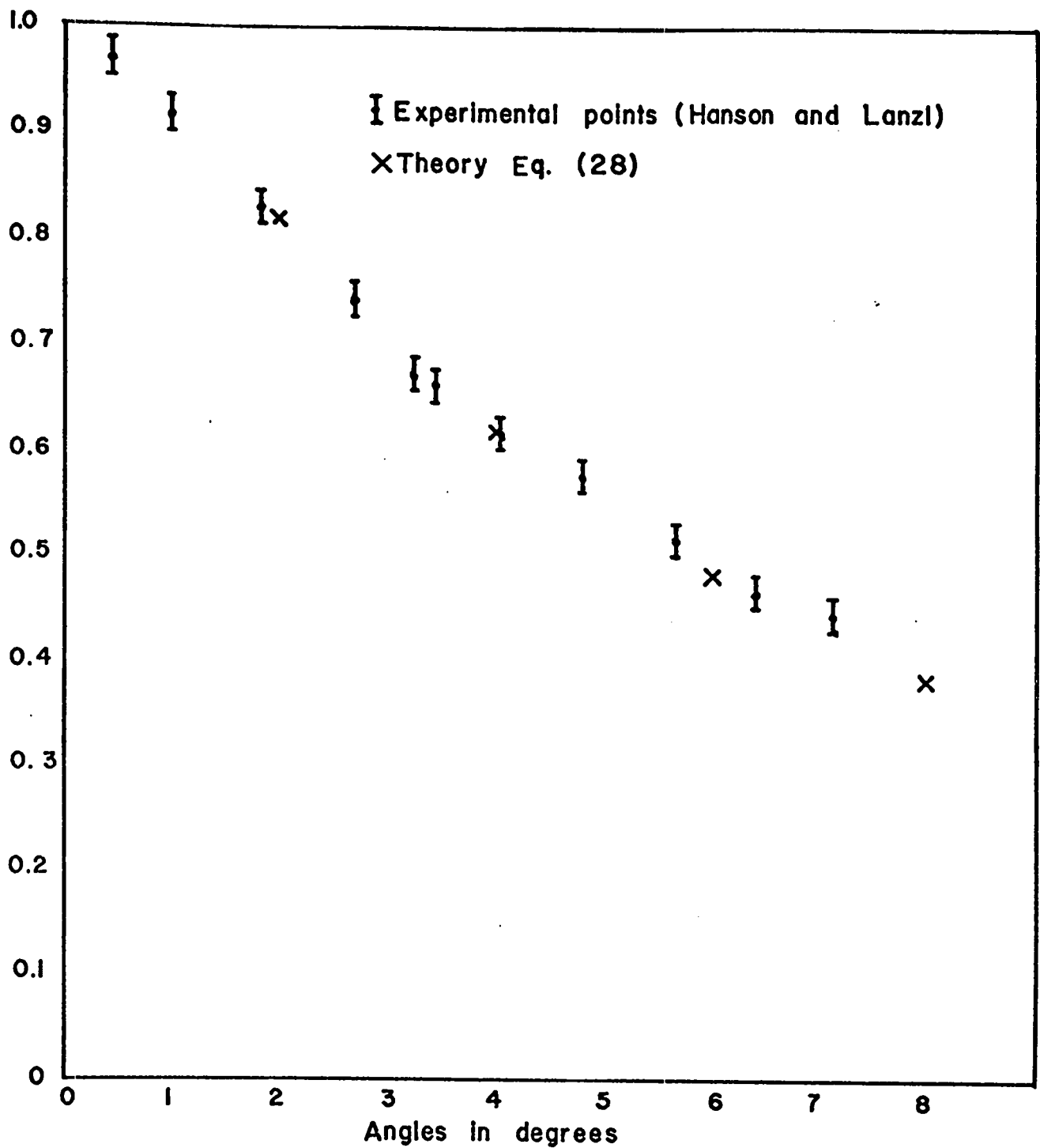


Fig. 12. Angular distribution. Ion chamber detector Au: 7250.7 mg/cm<sup>2</sup>.

Figure 13 is a plot of the central yield, as calculated by Eq. (95) indicating the experimental points of Lanzl and Hanson. The experimental and theoretical curves are normalized near the peak value. Again, the agreement is well within the experimental tolerances.

#### 4. Spectral Distribution.

Although there are no experimental data on the spectral distribution as a function of angle, it might be interesting to plot the intensity distribution that one could expect from a thick target. Using Eq. (85), the spectral distribution for a 7250.7 mg/cm<sup>2</sup> gold target is displayed in Fig. 14 for various angular positions. It is evident that the spectral distribution is essentially independent of angle, except for the high-energy tip.

### C. Summary

It has been demonstrated that the differential intensity from a target of any thickness can be represented by the equation

$$dI(k, t, \omega_0) = \frac{nNk}{\bar{a}} S_1(k, E_0) e^{-\mu(k)t} \left\{ \left[ \ln \left( 1 + \frac{\bar{a}t'}{1 + \omega_0} \right) - 2 \ln \left( 1 + \frac{D't'}{2} \right) \right] e^{D'(1 + \omega_0)/\bar{a}} - \frac{\omega_0}{2(1 + \omega_0)} \left[ 1 - \left( 1 + \frac{at'}{1 + \omega_0} \right)^{-2} \right] \right\} dk. \quad (96)$$

It is estimated that the error in Eq. (96) is a few percent. This equation assumes that the rays in the incident beam are parallel. Corrections can be accurately made for an incident beam having a Gaussian angular distribution in the manner developed in Chap. III, part B.

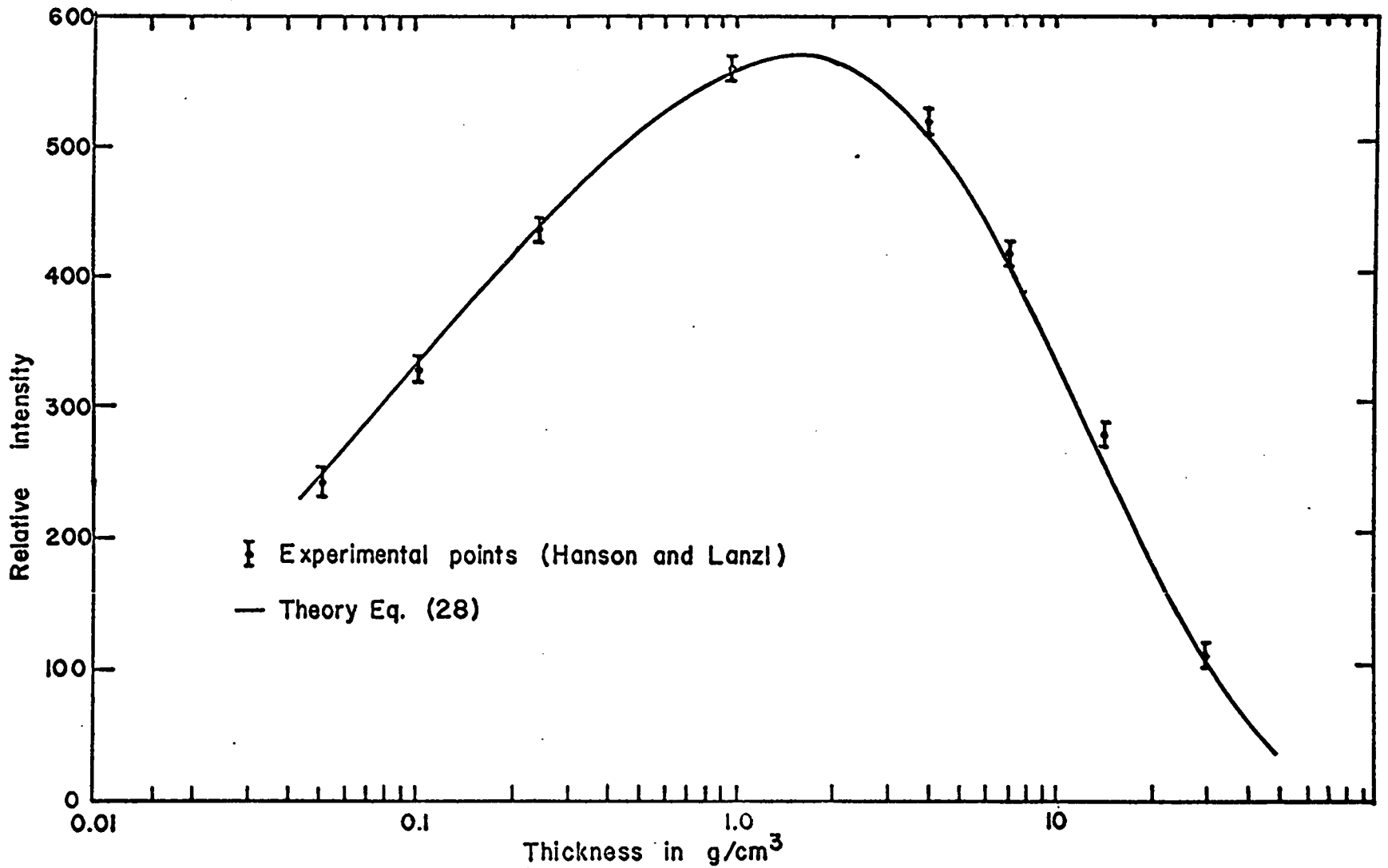


Fig. 13. Central yield vs target thickness.

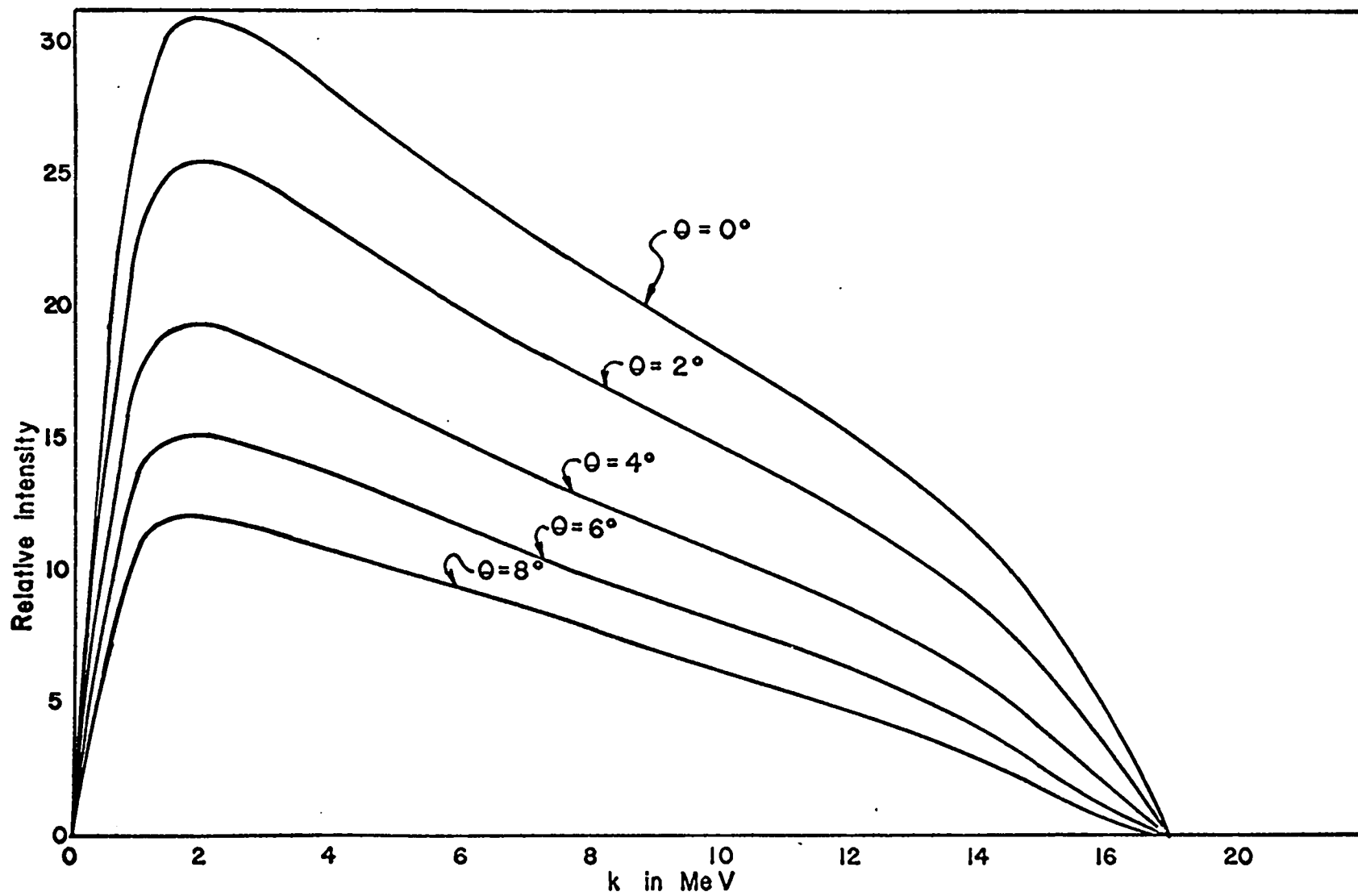


Fig. 14. Thick target bremsstrahlung for various angular positions, Au:  $7250.7 \text{ mg/cm}^2$ .

For most practical purposes, Eq. (96) can be simplified by letting  $D'$  be equal to zero. Thus, ignoring the second-order effects of the electron-energy gradient, absorption coefficient, and differential bremsstrahlung, Eq. (96) can be simplified to

$$dI(k, t, \omega_0) \approx \frac{nNk}{\bar{a}\rho} S_1(k, E_0) e^{-\mu(k)t} \left\{ \ln \left( 1 + \frac{\bar{a}t'}{1 + \omega_0} \right) - \frac{\omega_0}{2(1 + \omega_0)} \left[ 1 - \left( 1 + \frac{\bar{a}t'}{1 + \omega_0} \right)^{-2} \right] \right\} dk. \quad (96a)$$

The error in Eq. (96a) is estimated to be about 10 to 15%.

#### D. Thin Target Approximation

For thin targets Eqs. (96) and (96a) reduce to

$$\begin{aligned} dI(k, t, \omega_0)_{t \rightarrow 0} &\approx \frac{nNk}{\rho} \left\{ S_1(k, E_0) \frac{1}{(1 + \omega_0)^2} \right\} t \, dk \\ &= n \left\{ \frac{Nt}{\rho} \right\} k \sigma_s \, dk, \end{aligned} \quad (96b)$$

where  $n$  is the number of incident electrons,  $\frac{Nt}{\rho}$  is the number of atoms or scattering centers per  $\text{cm}^2$ , and  $k \sigma_s$  is Schiff's<sup>4</sup> bremsstrahlung cross section ( $\text{cm}^2$ ).

#### E. Thick Target Approximation

For most practical cases, the target thickness is chosen to produce optimum intensity. This is in the region where  $t > 1 \text{ gm/cm}^2$  for high- $Z$  material. In this range an approximate equation is

$$dI(k, t, \omega_0) \approx \frac{nNk}{\bar{a}\rho} S_1(k, E_0) e^{-\mu(k)t} \left\{ \ln \left( 1 + \frac{\bar{a}t'}{1 + \omega_0} \right) - \frac{\omega_0}{2(1 + \omega_0)} \right\} dk. \quad (96c)$$

The error is probably 10 to 20%.

APPENDIX A

B - Approximation

Molière's theory gives an equation defining the parameter B as:

$$B - \ln B = \ln \zeta^2 - 0.154. \quad (\text{A-1})$$

By inspection, the asymptotic value for B as  $\zeta \rightarrow \infty$  is  $B = \ln \zeta^2$ . Thus, assume

$$B = \ln \zeta^2 + \Delta(\zeta^2), \quad (\text{A-2})$$

and substitute back into (A-1) and solve for  $\Delta(\zeta^2)$ .

$$\Delta(\zeta^2) = \ln \left[ 0.8573 \{ \ln \zeta^2 + \Delta(\zeta^2) \} \right]. \quad (\text{A-3})$$

As  $\Delta(\zeta^2)$  is a very slowly varying function of  $\zeta^2$ , one can further assume that  $\Delta(\zeta^2)$  has the following form

$$\Delta(\zeta^2) = \ln \{ a \ln(b \zeta^2) \} \quad (\text{A-4})$$

or

$$B = \ln \left[ a \zeta^2 \{ \ln(b \zeta^2) \} \right]. \quad (\text{A-5})$$

Values for a and b are chosen to give a best fit to the values derived by Molière (Table A.I). The error of this approximation is less than 1% over the entire range.

TABLE A.I

Values of B									
	a = 1.1					b = 1.4			
$\zeta \rightarrow$	$10^1$	$10^2$	$10^3$	$10^4$	$10^5$	$10^6$	$10^7$	$10^8$	$10^9$
Molière	3.36	6.29	8.93	11.49	13.99	16.46	18.90	21.32	23.71*
Approximation	3.37	6.29	8.98	11.56	14.08	16.46	18.92	21.35	24.07

\*This value as tabulated by Segrè is probably in error.

APPENDIX B

Effective Depth of Bremsstrahlung Generation

Fortunately, as can be inferred from the derived weighting function  $W(x)$  (Fig. 1), the primary contribution to the detected bremsstrahlung is generated in the thin layer of target material facing the incident electron beam. The effective depth,  $\tau$ , can be approximately calculated by use of the weighting function  $W(x)$ .

Examination of  $W(x)$  and  $S_1(k, E_x)$  show

$$W(x) \approx (1 + ax)^{-1}, \quad (B-1)$$

and

$$\int_{k=0} S_1(k, E_x) dk \sim E_x^{3.5}.$$

If one arbitrarily defines the effective depth of bremsstrahlung,  $\tau$ , to be the depth at which one-half of the total detected intensity is generated, ignoring absorption, then

$$\int_{k=0}^{\tau} \frac{E_x^{3.5}}{1 + ax} dx = \int_{x=\tau}^{\infty} \frac{E_x^{3.5}}{1 + ax} dx. \quad (B-2)$$

It is assumed that  $E_x$  varies exponentially, which is a good approximation considering the thin layer in which most of the primary radiation is generated. Then

$$\int_{x=0}^{\tau} \frac{\exp\{-3.5ax\}}{1 + ax} dx = \int_{x=\tau}^{\infty} \frac{\exp\{-3.5ax\}}{1 + ax} dx. \quad (B-3)$$

Here  $\xi$  is the electron decay parameter as defined in Eq. (29).

Equation (B-3) can be directly reduced, that is,

$$2E_i \left[ -\left(\frac{1}{a} + \xi\right) 3.5\xi \right] = E_i \left[ -\left(\frac{1}{a}\right) 3.5\xi \right]. \quad (\text{B-4})$$

Because the arguments of these exponential integrals are both  $\ll 1$ ,

Eq. (B-4) can be simplified.

$$2 \left[ C + \ln \left\{ \left(\frac{1}{a} + \tau\right) 3.5\xi \right\} \right] \cong C + \ln \left\{ \frac{3.5\xi}{a} \right\} \quad (\text{B-5})$$

where  $C$  is Euler's constant, 0.5772.

Solving for the effective depth,

$$\tau \cong \left( \frac{1}{3.5 a \xi} \right)^{\frac{1}{2}} - \frac{1}{a}. \quad (\text{B-6})$$

Example: For tungsten,

$$\xi = 0.1956 \text{ cm}^2/\text{g} \text{ (value obtained from Venable}^{12} \text{ and Eq. (29))}$$

$$a = 165.3 \text{ cm}^2/\text{g}$$

$$C = \ln c = 0.5772$$

Therefore,  $\tau = 0.064 \text{ g/cm}^2$ .

## APPENDIX C

### Optimum Thickness

The optimum thickness target would be that thickness which produces the greatest intensity at the detector after passing through an object. As high-Z materials of considerable thickness have a minimum absorption cross section in the region of 3.5 MeV, it is desirable to calculate the target thickness that will give the maximum intensity at this energy. From the development of Eq. (54), the detected intensity is approximately proportional to

$$Q = e^{-\mu t} \left\{ \ln\left(1 + \bar{a}t/(1 + \omega_0)\right) - 2\ln\left(1 + Dt/2\right) \right\}. \quad (C-1)$$

The maximum intensity will occur when

$$\begin{aligned} \frac{dQ}{dt} = 0 = & \frac{\bar{a}}{(1 + \omega_0) + a\tau_0} - \frac{D}{1 + D\tau_0/2} \\ & - \mu \left\{ \ln\left[1 + a\tau_0/(1 + \omega_0)\right] - 2\ln(1 + D\tau) \right\} = V(\tau_0). \end{aligned} \quad (C-2)$$

The equation is solved by using Newton's approximations, knowing approximately the optimum thickness. Thus,

$$\tau_0 = t_0 - \frac{V(t_0)}{dV(t_0)/dt_0}, \quad (C-3)$$

where  $\tau_0$  is the optimum thickness, and  $t_0$  is an approximation. Should the first approximation be too great in error, the process may be iterated for increased accuracy.

Example: For tungsten at energy 3.49 MeV,  
 $a = 165.3 \text{ cm}^2/\text{g}$   
 $\Delta = 0.3717$   
 $\mu = 0.0408 \text{ cm}^2/\text{g}$   
 $t = 2.0 \text{ g/cm}^2$   
 $\omega_0 = 0.$

Using these parameters  $\tau_0 \cong 2.0746$ , by iteration  $\tau_0 \cong 2.0834$ .  
Therefore,  $\tau_0 = 2.08 \text{ g/cm}^2$ , which is equivalent to 0.1112 cm of tungsten.

Exponential Integral Approximation

The terms

$$\sum E_i = E_i \left[ \left( \frac{1}{a} + t' \right) (\Delta + \mu - 2\xi) \right] - E_i \left[ \left( \frac{1}{a} \right) (\Delta + \mu - 2\xi) \right] \quad (D-1)$$

can be expanded into

$$\begin{aligned} \sum E_i &= \ln \left| c \left( \frac{1}{a} + t' \right) (\Delta + \mu - 2\xi) \right| + \sum_{j=1}^{\infty} \frac{\left( \frac{1}{a} + t' \right)^j (\Delta + \mu - 2\xi)^j}{j! j} \\ &- \ln \left| c \left( \frac{1}{a} \right) (\Delta + \mu - 2\xi) \right| + \sum_{j=1}^{\infty} \frac{\left( \frac{1}{a} \right)^j (\Delta + \mu - 2\xi)^j}{j! j} \\ &= \ln(1 + at') + t'(\Delta + \mu - 2\xi) + \frac{\left( \frac{1}{a} + t' \right)^2 (\Delta + \mu - 2\xi)^2}{2! 2} \\ &- \frac{\left( \frac{1}{a} \right)^2 (\Delta + \mu - 2\xi)^2}{2! 2} + \dots \end{aligned} \quad (D-2)$$

However,  $1/a \ll t'$  except when  $t'(\mu + \Delta - 2\xi) \ll 1$ , again simplifying

$$\sum E_i = \ln(1 + at') + t'(\Delta + \mu - 2\xi) + \frac{(t')^2 (\Delta + \mu - 2\xi)^2}{2! 2} + \dots \quad (D-3)$$

or

$$\sum E_i = \ln(1 + at') + 2 \left\{ \frac{1}{2} t' (\Delta + \mu - 2\xi) + \frac{\frac{1}{4} (t')^2 (\Delta + \mu - 2\xi)^2}{2} + \dots \right\}.$$

The series in the brackets now appears as an approximation to the expansion of a logarithm function, thus

$$\sum E_i = \ln(1 + at') - 2\ln\left(1 + \frac{1}{2} t'(2\xi - \mu - \Delta)\right). \quad (D-4)$$

APPENDIX E

Useful Data

<u>Spectral Distribution</u>			<u>3.5 MeV Bremsstrahlung Intensity (Tungsten)</u>	
Photon Energy	Optimum Thickness Intensity*	Infinitely Thin Intensity**	Thickness	Intensity*
0.00 MeV	0.00	0.0419	0.00 g/cm <sup>2</sup>	0.00
0.49	3.99	0.2765	0.02	1.27
1.49	4.43	0.3806	0.04	1.75
2.49	4.31	0.4437	0.06	2.06
3.49	4.16	0.4861	0.10	2.46
4.49	3.99	0.5166	0.40	3.49
5.49	3.83	0.5399	0.80	3.90
6.49	3.67	0.5591	1.00	4.00
7.49	3.53	0.5781	1.20	4.06
8.49	3.40	0.5924	1.40	4.11
9.49	3.28	0.6086	1.80	4.15
10.49	3.17	0.6254	2.00	4.16
11.49	3.06	0.6431	<u>2.10</u>	<u>4.16</u> Optimum
12.49	2.96	0.6620	2.20	4.16
13.49	2.87	0.6824	2.40	4.15
14.49	2.78	0.7043	2.60	4.14
15.49	2.70	0.7278	3.00	4.11
16.49	2.60	0.7531	3.50	4.05
17.49	2.46	0.7801	4.00	3.99
18.49	2.32	0.8089	5.00	3.84
19.49	2.14	0.8395	6.00	3.69
20.49	1.92	0.8720	7.00	3.53
21.49	1.64	0.9064	<u>7.38</u>	<u>3.47</u> Maximum
22.49	1.26	0.9426	8.00	3.38 Electron
23.49	0.74	0.9807	9.00	3.24 Penetration
24.49	0.00	1.0000	10.00	3.12

\*Intensity in units of  $\frac{nNTE^2}{a\rho} m_0 c^2$

\*\*Intensity in units of  $\frac{nNTE^2}{a\rho} adx \cdot m_0 c^2$

Intensities will have the same dimensions as assumed for  $m_0 c^2$ .

## APPENDIX F

### Calculation of $\bar{a}$

To analytically calculate an average value of  $a(x)$  is very difficult. A calculation of  $\bar{a}$  in the region where  $p = 0.1$  will be considered sufficient. This is in the proper region of  $x$  that approximates the effective depth of generated bremsstrahlung (Appendix G). The value of  $\bar{a}$  allows the weighting function to be accurate to a few percent in the region where the weighting function contributes the greater part of the  $x$  integration.

Equation (79) is needed to calculate  $\bar{a}$ .

$$\bar{a} = 11.5K_2/\xi_e^2, \quad (\text{F-1})$$

where  $\xi_e^2$  is determined by

$$\xi_e^2 \ln \left\{ 1.1 \xi_e^2 \ln 1.4 \xi_e^2 \right\} = 5.20K_2/K_1. \quad (\text{F-2})$$

The easiest way to determine  $\bar{a}$  for the above equation is by graphical means. Figure 15 is a plot of the function given by Eq. (F-2). Using this graph, the value of  $\bar{a}$  for gold has a value  $166.9 \text{ cm}^2/\text{g}$ .

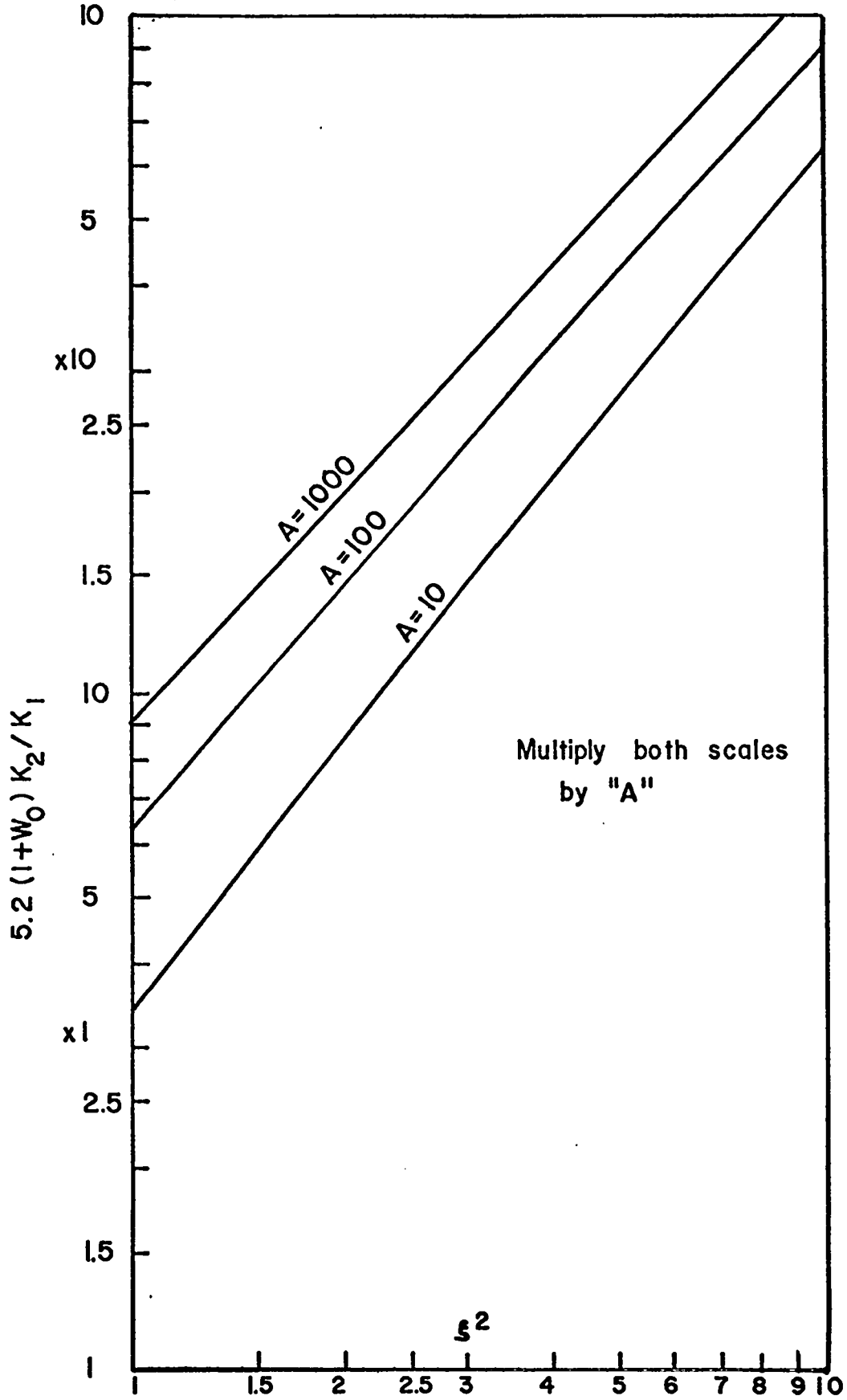


Fig. 15. Plot of  $\xi^2 \ln \{ 1.1 \xi^2 \ln 1.4 \xi^2 \}$ .

APPENDIX G

Effective Depth of Bremsstrahlung Generation

Following the pattern outlined in Chap. I (Appendix B), the effective depth of bremsstrahlung,  $\tau$ , is defined to be the depth at which approximately one-half of the total detected intensity is generated. The equation, which includes the effect of the angular displacement of the detector,  $\omega_0$ , is

$$\int_{x=0}^{\tau} \frac{\bar{a}e^{-3.5\xi x}}{1 + \omega_0 + \bar{a}x} dx - \left( \frac{\omega_0}{1 + \omega_0} \right) \int_{x=0}^{(1+\omega_0)/\bar{a}} \frac{\bar{a}e^{-3.5\xi x}}{1 + \omega_0 + \bar{a}x} dx$$

$$= \int_{x=\tau}^{\infty} \frac{\bar{a}e^{-3.5\xi x}}{1 + \omega_0 + \bar{a}x} dx. \quad (G-1)$$

$x=\tau$

The second term accounts for the resonance effect. The solution to this equation is obtained in a straightforward manner similar to that used in Chap. I.

$$\tau = \left( \frac{(1 + \omega_0)^2 \omega_0 / (1 + \omega_0)^{\frac{1}{2}}}{3.5 \xi \bar{c} \bar{a}} \right)^{\frac{1}{2}} - \frac{1 + \omega_0}{\bar{a}} \quad (G-2)$$

where  $\ln c = C = 0.5772$  (Euler's constant). Using the values of  $\bar{a}$  from Eq. F.I, the values of effective depth vs angular displacement for tungsten are tabulated in Table G.I. Practically the same values would be valid for gold.

TABLE G.I

EFFECTIVE DEPTHS FOR TUNGSTEN

$\omega_0 = 0$	1	4	9	16	25
$\tau = 0.06$	0.10	0.16	0.22	0.27	0.31

APPENDIX H

Nomenclature

$\bar{a}$	Roughly proportional to the mean square deflection gradient and is given by Eq. (23) and Eq. (79). Units: $\text{cm}^2/\text{g}$ .
$\alpha$	Reciprocal of the electron total energy squared $\alpha = E_x^{-2}$ .
$\beta$	A constant used in approximating the electron energy degradation in the target. $\beta$ is the slope of the electron differential energy loss vs incident kinetic energy curve.
$B, \theta_1^2$	Constants defined by Segre <sup>3</sup> to express details of the Molière theory for <b>particle</b> electron distribution, Eqs. (6), (10), and (11).
$C, c$	$C = \ln c = \text{Euler's constant} = 0.5772$ .
$d$	Distance of detector from target. Units: $\text{g}/\text{cm}^2$ .
$dx$	Differential thickness of target. Units: $\text{g}/\text{cm}^2$ .
$\delta$	Defined by $\delta = \theta_e^2 E_x^2 / (1 + \omega)$ .
$D$	Defined by $D = 2\xi - \mu(k) - \Delta(k)$ .
$D'$	Defined by $D' = \xi - \mu(k) - \Delta(k)$ .
$\Delta = \Delta(k)$	Related to bremsstrahlung gradient and given by Eq. (31) Units: $\text{cm}^2/\text{g}$ .
$E_0, E_x$	Total energy of the incident electrons and of the electrons at the penetration $x$ . Units: $m_0 c^2$ .
$\mathcal{E}_0, \mathcal{E}_x$	Kinetic energy of the incident electrons and of the electrons at the penetration $x$ . Units: $m_0 c^2$ .
$f(\theta_e, x, E_0)$	Fractional electron angular distribution, $f_m(\theta, x, \mathcal{E}_0)$ is Mott's <sup>2</sup> formula.
$\theta_e$	Angular displacement of the incident electron with respect to the axis. Units: radians.

$\theta_d$	Angular displacement of the emitted photon with respect to the axis between the direction of the electron and the photon. Units: radians.
$\theta_\gamma$	Angular displacement between the axial planes containing $\theta_e$ and $\theta_d$ . Units: radians.
$\theta$	Angular displacement between the axial planes containing $\theta_e$ when $\theta_d = \theta_e$ . Units: radians.
$k$	Photon energy. Units: $m_0 c^2$ .
$\mu(k)$	Linear absorption coefficient. Units: $\text{cm}^2/\text{g}$ .
$n$	Number of incident electrons.
$N$	Number of atoms in target. Units: $\text{atoms}/\text{cm}^3$ .
$\xi$	The electron energy loss gradient in the target, given by $\xi = \beta + (\sigma/\mathcal{E}_0)$ . Units: $\text{cm}^2/\text{g}$ .
$p$	Defined by $1/B\theta_1^2$ .
$p'$	Defined by $\alpha p$ .
$\rho$	Density of the target. Units: $\text{g}/\text{cm}^3$ .
$s$	Thickness of $s = t - x$ . Units: $\text{g}/\text{cm}^2$ .
$\sigma$	A constant used in approximating the electron energy degradation in the target. The zero energy intercept on the ordinate is $\sigma$ .
$S(k, x, \theta_d, E_0)$	Differential bremsstrahlung cross section. Units: $\text{cm}^2$ .
$t$	Thickness of the target. Units: $\text{g}/\text{cm}^2$ .
$t'$	The lesser of the following: $t$ , the thickness; or $\frac{1}{\beta} \ln \frac{\sigma + \mathcal{E}_0 \beta}{\sigma + k\beta}$ , the distance traveled by an electron in the target with initial kinetic energy $\mathcal{E}_0$ and emitting a photon of energy $k$ at the end of its range.
$\tau$	The effective depth for bremsstrahlung production. One-half bremsstrahlung intensity is produced at a depth less than

	$\tau$ , one-half at penetrations greater than $\tau$ . Units: $\text{g/cm}^2$ .
$\tau_0$	The optimum thickness. The depth of penetration at which the greatest intensity will be observed at the detector. Units: $\text{g/cm}^2$ .
$\phi$	Angular displacement between the axial planes containing $\theta_e$ and $\theta_d$ . Units: radians.
$W(x, E_0, \omega)$	Interpreted as the weighting function for the production of bremsstrahlung at a given angle at the depth $x$ per unit solid angle.
$x$	Thickness of the electron penetration depth.
$\omega_x$	Defined by $\omega_x = \theta_d^2 E^2$ , $\omega_0 = \theta_d^2 E_0^2$ .
$Z, z$	Atomic number of target material, of impinging particle (electron, $z = 1$ ).

### Acknowledgments

The author would like to acknowledge, with appreciation, the support received from LASL Group GMX-11 to this project, for the help received from Gary Massel for his calculation in the early phases of the program, and for interest and help received from M. E. Ennis throughout the development of this theory. The encouragement of Douglas Venable to produce this document in its present form is also appreciated.

## References

1. G. Molière, Z. Naturforsch 3a, 78 (1948).
2. N. F. Mott, Proc. Roy. Soc. (London) A124, 425 (1929); A126, 259 (1930); A135, 429 (1932).
3. E. Segrè, Experimental Nuclear Physics (John Wiley and Sons, Inc., New York, 1953).
4. L. I. Schiff, Phys. Rev. 83, 252 (1951).
5. A. Penfold, University of Illinois (unpublished data).
6. E. Hisdal, Phys. Rev. 105, 1821 (1957).
7. J. W. Motz, W. Miller, and H. O. Wyckoff, Phys. Rev. 89, 968 (1953).
8. L. H. Lanzl and A. O. Hanson, Phys. Rev. 83, 959 (1951).
9. J. D. Lawson, Nucleonics 10, (11) 61 (1952).
10. B. P. Nigam, M. K. Sundaresan, and Ta-You Wu, Phys. Rev. 115, 491 (1959).
11. Tables of Integral Transforms, A. Erdelyi, Ed., (McGraw-Hill, Inc., New York, 1954), Vol. 2, Chap. VIII, p. 15.
12. Douglas Venable, "PHERMEX: A Pulsed High-Energy Radiographic Machine Emitting X-Rays", LA-3241, Los Alamos Scientific Laboratory (May 15, 1967).